REPUBLIQUE ALGERIENNE DEMOCRATIQUE ET POPULAIRE
الجمهورية الجزائرية الديمقراطية الشعبية

MINISTRY OF HIGHER EDUCATION
AND SCIENTIFIC RESEARCH

HIGHER SCHOOL IN APPLIED SCIENCES
–T L E M C E N–

المدرسة العليا في العلوم التطبيقية
École Supérieure en
Sciences Appliquées

وزارة التعليم العالي والبحث العلمي

المدرسة العليا في العلوم التطبيقية
- تلمسان -

Mémoire de fin d'étude

Pour l'obtention du diplôme d'Ingénieur

Filière: Électrotechnique
Spécialité: Énergie et environnement

Présenté par : Hadj Abdelkader GUERMOUDI

Thème

Development of an Intelligent Prototype for Lithium Battery State of Charge Estimation

Soutenu publiquement, le 26/06/2023 , devant le jury composé de:

M. A. TAHOUR	Professeur	ESSA. Tlemcen	Président
M. A. F. KERBOUA	MCA	ESSA. Tlemcen	Directeur de mémoire
M. F. BOUKLI HACEN	Professeur	ESSA. Tlemcen	Co- Directeur de mémoire
M. A. CHELLAL	Doctorant	IPB. Portugal	Co- Directeur de mémoire
M. A. K. CHEMIDI	MCA	ESSA. Tlemcen	Examinateur 01
M. S. BELAROUCI	MCB	ESSA. Tlemcen	Examinateur 02

Année universitaire : 2022 /2023


بسم الله الرحمن الرحيم

Développement d'un prototype intelligent pour l'estimation de la charge des batteries au lithium

École Supèrieure en Sciences Appliquées de Tlemcen

Ingénieur en Electrotechnique - Énergie et Environnement

M. GUERMOUDI Hadj Abdelkader

2022-2023

To my dear parents, for their love, their sacrifices and their support in the most difficult moments, which are at the origin of our success, may GOD keep and protect them.

To my dear brothers, for their constant encouragement and all the help they give me on a daily basis.

To all the people who, from near or far, took part in this work.

I dedicate this humble work to them

Acknowledgements

First of all, I would like to thank Almighty and Merciful Allah, who has given me the strength and patience to accomplish this modest work.

The first person I would like to thank most sincerely is my supervisor ***Pr. A. KERBOUA***, Senior Lecturer at ESSA Tlemcen, for all his efforts, his consistent help and the trust he places in me on a daily basis, without which this work would not have been possible. He was always there to give me good advice.

I would also like to express my gratitude to Professor ***Pr. F. BOUKLI HACEN*** for his invaluable contribution to this work. His innovative ideas and dedication have greatly enriched my project. Working with him was a real pleasure, and I'm grateful for his close collaboration and support throughout the process. His presence and commitment were an undeniable source of motivation.

I would also like to express my gratitude to ***Pr. A. CHELAL*** and ***Pr. L. MERAD*** for their invaluable contribution to this work. Their in-depth knowledge and expertise were of great added value to my project. Their support and sound advice have greatly contributed to its success. I am grateful to have had the opportunity to collaborate with such competent and committed professionals.

I would also like to thank ***Pr. A. Tahour***, Professor at ESSA Tlemcen, for agreeing to chair the jury.

My sincere thanks also go to the members of the jury ***Pr. A.K. Chemidi***, Senior Lecturer at ESSA Tlemcen and ***Pr. S. Belarouci***, Assistant Lecturer at ESSA Tlemcen for their interest in my study and for agreeing to examine my work and enrich it with their proposals.

Résumé

La technologie des batteries est l'un des goulets d'étranglement des voitures électriques. Que ce soit en théorie ou en pratique, la recherche sur la gestion des batteries est extrêmement importante, en particulier pour l'estimation de l'état de charge des batteries. En fait, la batterie possède de fortes propriétés non linéaires et variables dans le temps, qui sont extrêmement complexes. Par conséquent, l'estimation précise de l'état de charge est une tâche difficile.

Dans cette étude, une analyse complète a été menée pour explorer la popularité et les avantages des piles au lithium, ainsi que leurs caractéristiques et les facteurs influençant les mesures de l'état de charge. L'objectif était de développer un circuit intégré précis d'estimation de l'état de charge qui pourrait répondre à des exigences spécifiques et fournir des informations sur le comportement des cellules au lithium.

Les résultats de l'étude contribuent non seulement au domaine des systèmes de gestion des batteries, mais offrent également une compréhension plus large de l'estimation de l'état de charge des cellules au lithium. En mettant en œuvre un modèle passif sur un circuit électronique avec microcontrôleur, le circuit permet une mesure précise et en temps réel de l'état de charge.

Mots-Clés: État de charge ; système embarqué ; batterie au lithium ; système embarqué ; intelligence artificielle ; capteurs.

الـمـلـخص

تعتبر تكنولوجيا البطارية أحد العوائق في السيارات الكهربائية. سواء في النظرية أو في العملية، فإن البحث في إدارة البطارية أمر مهم للغاية، خاصة في تقدير حالة شحن البطارية. في الواقع، تتمتع البطارية بخصائص غير خطية ومتغيرة مع الزمن، مما يجعل عملية تقدير حالة الشحن بالغة التحدي.

في هذه الدراسة، تم إجراء تحليل شامل لاستكشاف شعبية ومزايا الخلايا الليثيوم، بالإضافة إلى خصائصها والعوامل التي تؤثر في قياس حالة الشحن. كان الهدف هو تطوير دائرة مضمنة دقيقة لتقدير حالة الشحن التي يمكن أن تلبي المتطلبات المحددة وتوفر رؤى حول سلوك الخلايا الليثيوم.

من خلال تحليل نظرية الشبكات العصبية وإجراء تجارب شاملة ، نهدف إلى تحسين دقة تقدير حالة الشحن. ينصب تركيزنا على فهم العلاقة المعقدة بين متغيرات الإدخال و حالة الشحن، وتسخير قوة الشبكات العصبية لالتقاط هذه العلاقة ونمذجتها بشكل فعال.

تسهم نتائج الدراسة ليس فقط في مجال أنظمة إدارة البطاريات، ولكنها توفر فهما أوسع لتقدير حالة الشحن للخلايا الليثيوم. من خلال تنفيذ نموذج قائم على المراقبة على دائرة إلكترونية مع متحكم صغير الحجم، تمكن الدائرة من قياس حالة الشحن بدقة وفي الوقت الحقيقي.

الكلمات الرئيسية: حالة الشحن، بطارية الليثيوم، الذكاء الاصطناعي، الحساسات .

Abstract

Battery technology has been one of the bottlenecks in electric cars. Whether it is in theory or in practice, the research on battery management is extremely important, especially for battery state of charge estimation. In fact, the battery has a strong time-varying and non-linear properties, which are extremely complex. Therefore, accurately estimating the state of charge is a challenging task.

In this study, a comprehensive analysis was conducted to explore the popularity and advantages of lithium cells, along with their characteristics and the factors influencing state of charge measurements. The aim was to develop an accurate embedded state of charge estimation circuit that could meet specific requirements and provide insights into the behavior of lithium cells.

The study's results contribute not only to the field of battery management systems but also offer a broader understanding of state of charge estimation for lithium cells. By implementing a passive-based model on an elecronic circuit with microcontroller, the circuit enables real-time and precise measurement of the state of charge.

Keywords: State of Charge; Embedded system; Lithium Battery; Embedded system; Artificial Intelligence; Sensors.

Contents

General Introduction **1**

1 State of the Art Battery Technologies **3**

1.1 Introduction 3

1.2 Overview of Lithium-ion Battery 4

1.3 Batteries Characteristics 6

1.3.1 Nominal Voltage 6

1.3.2 Capacity 6

1.3.3 Internal Resistance 6

1.3.4 Life Cycle 6

1.3.5 Charge/Discharge Rate 7

1.3.6 Operating Temperature 7

1.4 Performance Comparison "Lithium-Ion Battery and Others" 7

1.5 Types of Lithium Cells 8

1.5.1 Lithium Cobalt Oxide(LiCoO2) — LCO 8

1.5.2 Lithium Manganese Oxide (LiMn2O4) — LMO 9

1.5.3 Lithium Nickel Manganese Cobalt Oxide (LiNiMnCoO2) — NMC . 9

1.5.4 Lithium Iron Phosphate (LiFePO4) — LFP 9

1.5.5 Lithium Nickel Cobalt Aluminum Oxide (LiNiCoAlO2) — NCA . . 9

1.5.6 Lithium Titanate (Li2TiO3) — LTO 10

1.6 States of Batteries 11

1.6.1 State of Charge . . . 11
1.6.2 State of Health . . . 14
1.6.3 State of function . . . 16
1.7 Battery Management System . . . 17
1.8 Conclusion . . . 19

2 Advanced SOC Estimation Techniques: From Traditional Methods to FNN Adaptation 20

2.1 SOC Estimation Methods . . . 20
2.1.1 Methods Based on Direct Measurement . . . 21
2.1.2 Book-keeping Method . . . 23
2.1.3 Methods Based on Adaptive Systems . . . 24
2.1.4 Hybrid Methods . . . 28
2.2 Adopted Method: Feed Forward Neural Network . . . 29
2.2.1 Experimental Procedure: Supervised BP Learning . . . 29
2.2.2 Dataset Selection and Data Preprocessing . . . 30
2.2.3 Neural Network Model Training . . . 32
2.2.4 Noise Elimination Using Moving Average Filter . . . 35
2.3 Conclusion . . . 37

3 Design and Implementation 38

3.1 Introduction . . . 38
3.2 Programming Language . . . 38
3.3 Software and Programming Tools . . . 39
3.3.1 Arduino Software . . . 39
3.3.2 ISIS Proteus Software . . . 39
3.3.3 Matlab Coder . . . 40
3.4 Electronic circuit . . . 40
3.4.1 Electrical Components . . . 40
3.4.2 Circuit on Breadboard . . . 44

3.5 Conclusion 45

4 Implementation and Results **47**

4.1 Introduction 47

4.2 LG HG2 cell Model 48

4.2.1 Results 48

4.2.2 Analyzing and Discussion 50

4.3 CGR18650CG Model 51

4.3.1 Model Training and SOC Estimation 52

4.3.2 Analyzing and Discussion 58

4.4 Conclusion 59

Conclusion Générale et Perspectives **61**

A Conceptual Implementation Arduino Code **A1**

B SOC Predicting Function **B1**

List of Tables

1.1 Comparison of Battery Types [2]. 8
1.2 Comparison of different lithium-ion battery chemistries [13]. 10

2.1 Data Information 31
2.2 FNN model properties 32

3.1 Characteristics of Panasonic CGR18650CG Lithium Cell [17]. 40
3.2 Characteristics of Arduino Mega2560 41

List of Figures

1.1 Charge, discharge mechanism of a lithium-ion battery [6]. 5
1.2 Comparison between different types of cathodes [14] 11
1.3 Internal resistance variation for different discharge currents and different SOC levels [17]. 13
1.4 OCV–SOC curves between 30% and 80% SOC at different temperatures for Panasonic CGR18650CG [17]. 14
1.5 Synoptic diagram of a BMS 18

2.1 Experimental OCV-SOC curve for LFP cell [28]. 22
2.2 The architecture of the SOC estimating FNN [28]. 25
2.3 RC complex ECM for lithium cell [1] 27
2.4 RC complex equivalent electrical model in MATLAB Simulink 27
2.5 Experimental Procedure 30
2.6 Training data plot 32
2.7 Regression Plot 33
2.8 Training State 34
2.9 Estimated Values vs real values 35
2.10 Filtered values using MAF 36
2.11 Error between Filtered SOC values and actual SOC 36

3.1 CCCV charging curve for TP4056 [42] 43
3.2 Voltage Measurement Circuit 44
3.3 Discharge Test Circuit 45

4.1 CGR18650CG testing data 48
4.2 Estimated SOC by LG HG2 model 49
4.3 Error using LG HG2 model 50
4.4 Constant Current Discharge Test for CGR18650CG Cell 52
4.5 Mean Square Error 53
4.6 Training State 53
4.7 Regression Plot 54
4.8 Predicted SOC vs Calculated SOC for CGR18650CG Model 55
4.9 Error between Predicted and Calculated SOC 56
4.10 Filtered SOC vs Calculated SOC for CGR18650CG Model 57
4.11 Error between Filtered and Calculated SOC 58

Abbreviation

This document contains a number of abbreviations which we define here.

SOC	State of Charge
SOF	State of Function
SOH	State of Health
BP	Backpropagation
BMS	Battery Management System
RBF	Radial Basis Function
SVM	Support Vector Machine
OCV	Open Circuit Voltage
FNN	Feed Forward Neural Network
ANN	Artificial Neural Network
EV	Electrical Vehicles
ECM	Equivalent Circuit Model
UDDS	Urban Dynamometer Driving Schedule
HWFET	Highway Fuel Economy Test
US06	High acceleration aggressive driving schedule
CCCV	Constant Current Constant Voltage

CSV	Comma Separated Values
LCO	Lithium Cobalt Oxide
LMO	Lithium Manganese Oxide
NMC	Nickel Manganese Cobalt Oxide
NCA	Lithium Nickel Cobalt Aluminium Oxide
LFP	Lithium Iron Phosphate
LTO	Lithium Titanate
LMO	Lithium Manganese Oxide
SGD	Stochastic Gradient Descent
Adam	Adaptive Moment Estimation
MSE	Mean Square Error
MAE	Mean Absolute Error
MAF	Moving Average Filter

Symbols

$	Dollar
A	Ampere
Ah	Ampere-hour
mAh	Milliampere-hour
C	Celsius
mA	Milliamperes
V	Volt
Wh	Watt-hour
W	Watt
KWh	Kilo-Watt-hour
Ω	Ohm
mΩ	Milliohms
kg	kilogram

General Introduction

Due to technological advancements and the growing demand for electric vehicles and portable electronics, lithium batteries have gained immense popularity. This is primarily attributed to their remarkable attributes of high energy density and long cycle life. However, accurately determining the state of charge (SOC) of lithium cells has emerged as a notable challenge. The SOC of a battery denotes the amount of available energy, and having precise knowledge of this parameter is critical for optimizing battery utilization, preventing over-discharge or over-charge situations, and ensuring efficient and reliable operation.

The repercussions of inaccurate SOC estimation are far-reaching and include diminished performance, shortened battery lifespan, and potential safety risks. Consequently, the development of dependable SOC estimation methods for lithium cells has attracted significant attention from both the research and industrial sectors. By addressing this issue, we can enhance the usability, efficiency, and safety of lithium-based systems, which in turn propels the advancement of sustainable energy storage technologies.

Our project is dedicated to addressing the intricate task of precisely estimating the state of charge in lithium cells. To accomplish this, we harness the characteristics and behavior of these batteries and employ artificial intelligence (AI) techniques. Given the intricate and ever-changing nature of lithium cells, we propose utilizing neural networks, a potent AI tool, to construct SOC estimation models. We investigate three distinct neural network architectures to determine the most efficient approach. By training these models on an extensive dataset encompassing the behavior of lithium cells, we strive to attain a remarkable level of accuracy.

This document is made up of four (04) chapters, the first of which gives a general presentation of lithium cells, their types and characteristics, as well as a presentation of the problems involved in state-of-charge estimation. The second chapter is devoted to the state of the art of state-of-charge estimation methods highlighting the adopted method. The third chapter presents the necessary software and hardware needed for the experiments. The fourth chapter shows the results of the experiments and results comparison, as well as the validation of the hypotheses.

Chapter 1

State of the Art Battery Technologies

1.1 Introduction

Over the past few years, significant progress has been made in the realm of rechargeable batteries, revolutionizing their design and technology. One of the most prevalent and widely used types is the lithium-ion battery, commonly found in portable electronic devices such as smartphones, robots, and electrical vehicles. These batteries boast a remarkable energy density, enabling them to store a substantial amount of power in a compact and convenient form. Compared to other rechargeable battery options, lithium-ion batteries also exhibit an impressive lifespan, ensuring their longevity. Additionally, they are lightweight and possess a low self-discharge rate, meaning they can retain their charge for extended periods when not in use [1].

Another variant of rechargeable battery is the nickel-metal hybrid battery, predominantly employed in hybrid and electric vehicles. These batteries excel in terms of capacity, surpassing that of lithium-ion batteries, and are highly resistant to damage caused by overcharging. However, it is worth noting that nickel-metal hybrid batteries tend to be heavier and more costly compared to their lithium-ion counterparts [2].

Beyond these established technologies, researchers are actively exploring newer alternatives in the field of rechargeable batteries. Solid-state batteries, for example, employ solid electrolytes instead of liquid ones, boasting the potential for enhanced safety measures and higher energy densities in comparison to traditional lithium-ion batteries. Moreover, the scientific community is pushing the boundaries by investigating batteries that utilize innovative materials like silicon, graphene, and lithium-sulfur. These materials hold tremendous promise in terms of significantly improving the performance and lifespan of rechargeable batteries [3].

The realm of rechargeable batteries is an ever-evolving and constantly improving field, with ongoing developments and innovative breakthroughs. With relentless advancements and new discoveries on the horizon, it is anticipated that rechargeable battery technologies will become even more efficient and effective in the years to come.

1.2 Overview of Lithium-ion Battery

By the end of the 1900s, the battery stood as the sole power source due to the absence of power generators and grid supplies. Over time, this technology has undergone continuous development, leading to the emergence of various battery types [4]. One commonly used variant was the "wet cells", which consisted of open containers holding liquid electrolytes and metallic electrodes. These batteries could be reused by substituting their materials, although they lacked portability, which made them suitable for early Electric Vehicles (EV) that utilized semi-sealed wet cells [2].

During the early stages of battery technology, assembled batteries produced current but were unable to be electrically recharged once the active elements were depleted. A significant breakthrough occurred with the invention of the lead-acid battery, which introduced rechargeable types capable of replenishing electric energy. These batteries could store energy repeatedly, thereby extending their lifespan. In contrast, the disposable Li-ion battery gained popularity in the rechargeable battery market due to its high energy density and long lifespan, despite its relatively high unit price [2].

The structure of Li-ion batteries comprises two electrodes, namely the anode and the cathode, which are divided by a separator. An electrolyte is present in the separator, allowing lithium ions to migrate from the cathode to the anode during the charging process and reverse their movement during discharging, as depicted in Figure 1.1. In contrast to non-rechargeable batteries that incorporate metallic lithium, Li-ion batteries employ a compound lithium electrode material [5].

In EV applications, Li-ion batteries have gained popularity as a portable rechargeable alternative to lead-acid batteries, primarily due to their lightweight nature and high energy density [4]. Despite their advantageous properties, Li-ion batteries require stringent testing conditions and careful handling during manufacturing and usage due to the flammable nature of their electrolyte. Thus precautions are necessary to prevent accidents and failures [4].

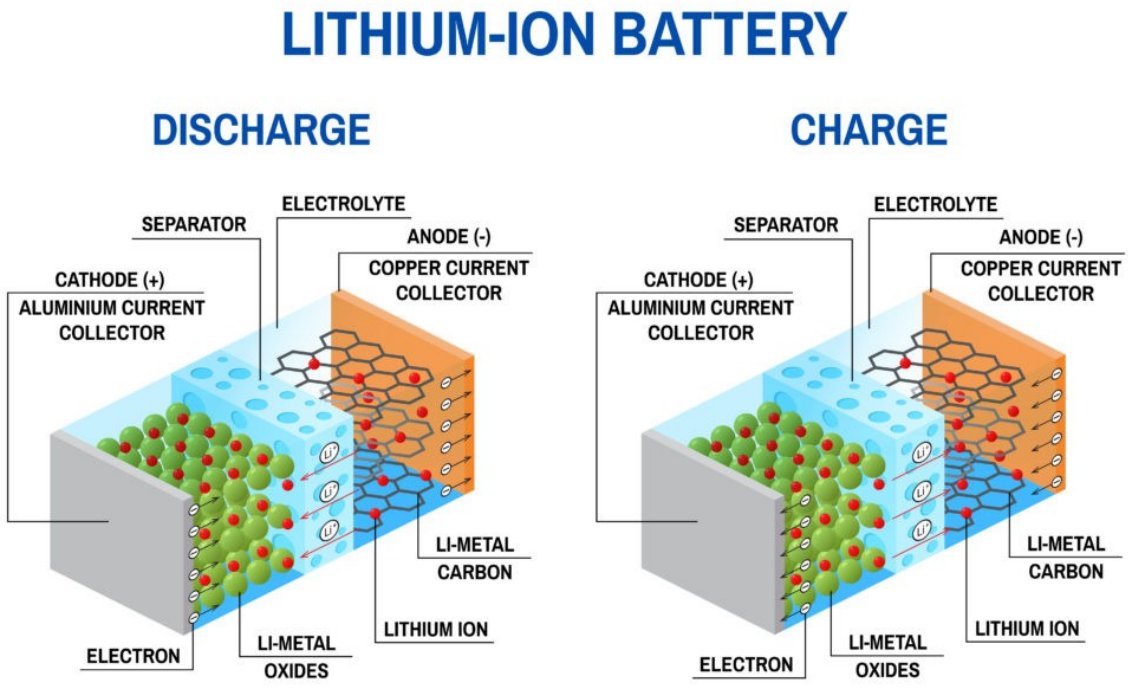

Figure 1.1: Charge, discharge mechanism of a lithium-ion battery [6].

1.3 Batteries Characteristics

1.3.1 Nominal Voltage

The nominal voltage of a battery varies according to the technology for which it has been developed. It depends on the nature and concentration of the chemical species present in the in the battery. Its value is only an average, since at the start of a discharge, the voltage is higher, and as the discharge progresses, the voltage drops [7].

1.3.2 Capacity

The capacity of a lithium cell refers to its ability to store and deliver electrical energy. It is typically measured in ampere-hours (Ah) or milliampere-hours (mAh). The capacity indicates how much charge the cell can hold and how long it can power a device. For instance, if a lithium cell has a capacity of 2000mAh, it can theoretically supply a current of 2000 mA for one hour.

1.3.3 Internal Resistance

The internal resistance of a battery is a disadvantageous characteristic because it causes the voltage at its terminals to drop as the current it delivers increases. This value is partly due to internal connections, chemical reaction inertia, built-in protection circuits, and the aging state of the battery. As a result, internal resistance is an important parameter in quantifying a battery's SOH. Its value is generally a few hundred milliohms (mΩ) [8].

1.3.4 Life Cycle

The life cycle of a battery represents the total number of charge-discharge cycles it can endure before reaching the end of its useful lifespan. it is an essential factor to consider as it directly affects the overall longevity of the battery. Batteries with a high cycle life can withstand numerous charge-discharge cycles before requiring replacement, whereas batteries with a low life cycle may need to be replaced more frequently [4].

1.3.5 Charge/Discharge Rate

The rate, also known as the C-rate, at which a battery can be charged or discharged is referred to the charge/discharge rate, commonly measured in amperes (A), for example 1C refers to 3A discharge current in 3000 mAh battery. Significantly impacts both the overall performance and lifespan of a battery. Charging a battery too rapidly can lead to a reduced lifespan, while discharging it too quickly can result in diminished performance. Therefore, maintaining an appropriate C-rate is important for optimizing the efficiency and longevity of the battery.

1.3.6 Operating Temperature

This refers to the range of temperatures over which a battery can be used without damage or significant loss of performance. The operating temperature of a battery can have a significant impact on its performance and lifespan, as high temperatures can result in decreased performance and decreased lifespan, while low temperatures can result in decreased performance [9].

1.4 Performance Comparison "Lithium-Ion Battery and Others"

Various conventional batteries, including lead-acid [10], nickel-cadmium (Ni-Cd) [11], and nickel-metal hydride (Ni-MH) [12], have been developed. When compared in Table 1, Li-ion batteries outperform other types in terms of energy efficiency, power density, compact design, wide temperature range, fast charging, long cycle life, low self-discharge, and high efficiency in energy, charge, and voltage [2]. These desirable features have made Li-ion batteries the preferred choice in commercial markets, powering bio-implanted devices, medical instruments, and portable electronics. Table 1.1 shows a comparison between this 4 types of batteries.

Table 1.1: Comparison of Battery Types [2].

Battery Type	Li-ion	Ni-Cd	Lead-acid	Ni-MH
Energy Density (Wh/kg)	110-160	45-80	30-50	60-120
Power Density (W/kg)	1800	150	180	250-1000
Nominal Voltage (V)	3.6	1.25	2	1.25
Cycle Life (cycles)	500-1000	1500	200-300	300-500
Overcharge Tolerance	Very Low	Moderate	High	Low
Self Discharge	Very Low	Moderate	Low	High
Thermal Stability	Most Stable	Least Stable	Least Stable	Least Stable

1.5 Types of Lithium Cells

Typically, the primary sources of active lithium ions in a battery are the cathode or positive electrode material. To achieve a high capacity, a significant amount of lithium is incorporated into this material. Moreover, cathode materials undergo a reversible process where they exchange lithium ions, accompanied by slight structural modifications that affect their properties. In the electrolyte, materials are formulated using reasonably-priced high lithium ion content, which ensures good diffusivity, conductivity, and efficiency [36]. Common cathode materials include Lithium Cobalt Oxide (LCO), Lithium Manganese Oxide (LMO), Lithium Iron Phosphate (LFP), Lithium Nickel-Manganese-Cobalt Oxide (NMC), Lithium Nickel Cobalt Aluminium Oxide (NCA), and Lithium Titanate (LTO) [3].

1.5.1 Lithium Cobalt Oxide(LiCoO2) — LCO

LCO is a popular choice for mobile phones, laptops, and digital cameras due to its high specific energy. The battery is made up of a cobalt oxide cathode and a graphite carbon anode, with lithium ions moving from the anode to the cathode during discharge and reversing during charge. However, LCO has a relatively short lifespan, low thermal stability, and limited load capabilities. Newer systems include nickel, manganese, and/or aluminum to improve performance and reduce cost. Li-cobalt should not be charged or discharged at a current higher than its C-rating to avoid overheating and stress.

1.5.2 Lithium Manganese Oxide (LiMn2O4) — LMO

LMO is a Li-ion cell that improves ion flow and has low internal resistance, enabling fast charging and high-current discharging. LMO has high thermal stability and enhanced safety, but limited cycle and calendar life. It has roughly one-third lower capacity than Li-cobalt but can be optimized for longevity, maximum load current or high capacity. LMO is used for power tools, medical instruments, and hybrid and electric vehicles.

1.5.3 Lithium Nickel Manganese Cobalt Oxide (LiNiMnCoO2) — NMC

NMC is a successful Li-ion system that can serve as Energy Cells or Power Cells. NMC combines nickel and manganese to enhance their respective strengths and cobalt stabilizes nickel. The cathode combination typically consists of one-third each of nickel, manganese, and cobalt. NMC is used in power tools, e-bikes, and electric powertrains. Its capacity and discharge current can be optimized for specific power or energy.

1.5.4 Lithium Iron Phosphate (LiFePO4) — LFP

LFP has a lower nominal voltage of 3.2V/cell, making its specific energy lower than cobalt-blended lithium-ion. It is more tolerant to full charge conditions and elevated temperatures, but has a higher self-discharge and requires cleanliness in manufacturing. Li-phosphate is often used as a lead acid starter battery replacement and can be topped up while driving, but overcharging for a prolonged time can stress the battery. Cold temperature can also affect performance and cranking ability.

1.5.5 Lithium Nickel Cobalt Aluminum Oxide (LiNiCoAlO2) — NCA

NCA has high specific energy, good specific power, and a long life span, but is less safe and more expensive compared to other lithium-ion batteries.

1.5.6 Lithium Titanate (Li2TiO3) — LTO

LTO batteries replace graphite in the anode with a spinel structure, have a nominal voltage of 2.40V, and can be fast charged with a high discharge current of 10C. They are safe, have excellent low-temperature discharge characteristics, and have a higher cycle count than regular Li-ion batteries. While they have thermal stability under high temperature, they are expensive and have a low specific energy of 65Wh/kg. They are used in electric powertrains, uninterruptible power supply, and solar-powered street lighting.

Table 1.2, and Figure 1.2 represents a general comparison between different lithium-ion battery chemistries.

Table 1.2: Comparison of different lithium-ion battery chemistries [13].

	Operating Voltage (V)	**Energy** (Wh/kg)	**Charge** (C)	**Discharge** (C)	**Cycle Life** (cycles)	**Cost** ($/kWh)
LCO	3.0-4.2	150-200	0.7C-1C	1C	500-1000	200
LMO	3.0-4.2	100-150	0.7C-1C	1C-10C	1000	150
NMC	3.0-4.2	150-220	0.7C-1C	1C-2C	1000	420
LFP	2.5-3.65	90-120	1C	1C-25C	2000	580
NCA	3.0-4.2	200-260	0.7C	1C	500	350
LTO	1.8-2.85	50-80	1C-5C	10C	3000-7000	1,005

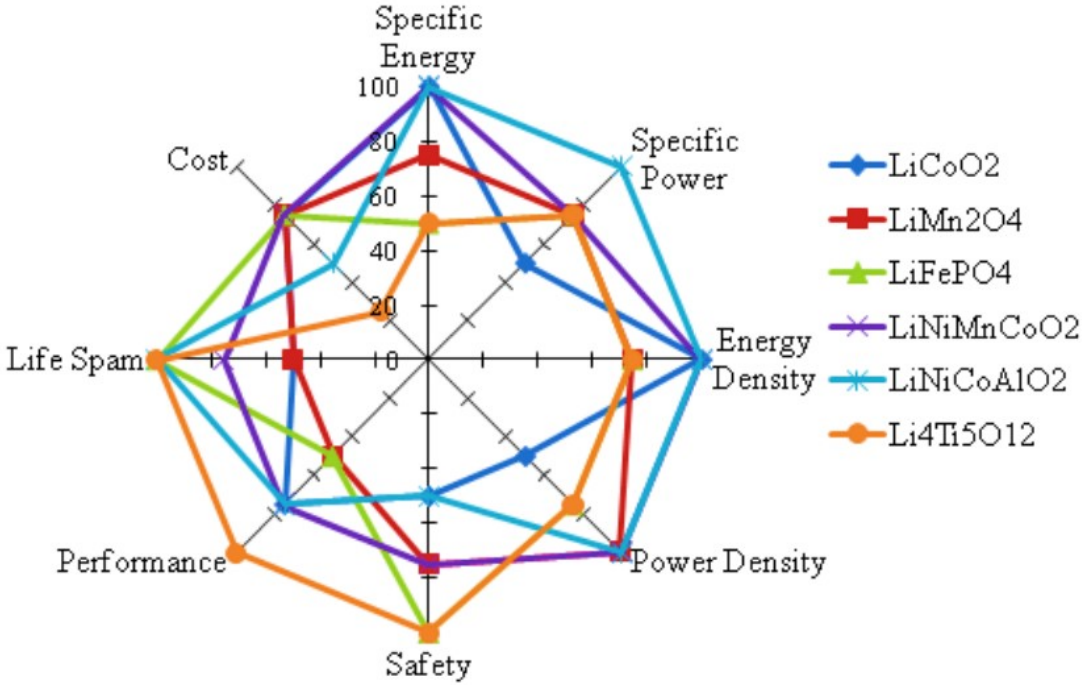

Figure 1.2: Comparison between different types of cathodes [14]

.

1.6 States of Batteries

1.6.1 State of Charge

SOC is one of the most important parameters for batteries, but its definition presents many different issues. In general, the SOC of a battery is defined as the ratio of its current capacity the nominal capacity, which is given by the manufacturer and represents the maximum amount of charge that can be stored in the battery [1]. The SOC can be defined as follows:

$$SOC = \frac{Q_{used}}{Q_{rated}} \times 100\% \tag{1.1}$$

where SOC is the State of Charge, Q_{used} is the amount of charge discharged from the battery, and Q_{rated} is the rated capacity of the battery.

The accurate estimation of SOC remains a significant challenge in battery usage. A

precise SOC estimation provides information about the remaining capacity, enabling the application to implement efficient control strategies for energy conservation, protection against over-discharge which means enhancement of battery lifespan. However, a battery functions as a source of chemical energy storage, and the chemical energy cannot be directly measured, which poses a challenge in estimating the state of charge. The complexity of accurately estimating the SOC stems from limitations in battery models and parametric uncertainties. These limitations result in instances of low accuracy and unreliable SOC estimates in practical applications [15].

Open Circuit Voltage

The open Circuit Voltage (OCV) of a battery cell is the potential difference between the positive electrode and the negative electrode when no current flows and the electrode potentials are at equilibrium. A battery undergoing charge or discharge does not exhibit this potential since it is modified by kinetic effects. Open circuit voltage, as a nonlinear function of state of charge of lithium ion battery, commonly obtained through offline OCV test at certain ambient temperatures and aging stages. The OCV-SOC relationship may be inaccurate in real application due to the difference in operation conditions [7].

Discharge Current

The discharge current has a direct effect on the internal resistance of a lithium cell, which in turn affects the measurement of SOC. As the discharge current increases, the internal resistance of the battery also increases. This increased resistance leads to a higher voltage drop across the battery during discharge [16].

When measuring SOC based on voltage, the voltage drop caused by the internal resistance can result in an underestimation of the actual SOC. This is because the measured voltage will be lower than expected due to the voltage drop across the internal resistance. To accurately measure SOC, it is important to account for the influence of discharge current on the internal resistance. This can be done by implementing compensation techniques or using advanced algorithms that consider the dynamic behavior of the battery's

internal resistance during discharge. By taking into account the discharge current and its impact on the internal resistance, more accurate SOC measurements can be obtained [16]. Figure 1.3 shows the effect of internal resistance on terminal voltage at different discharge currents .

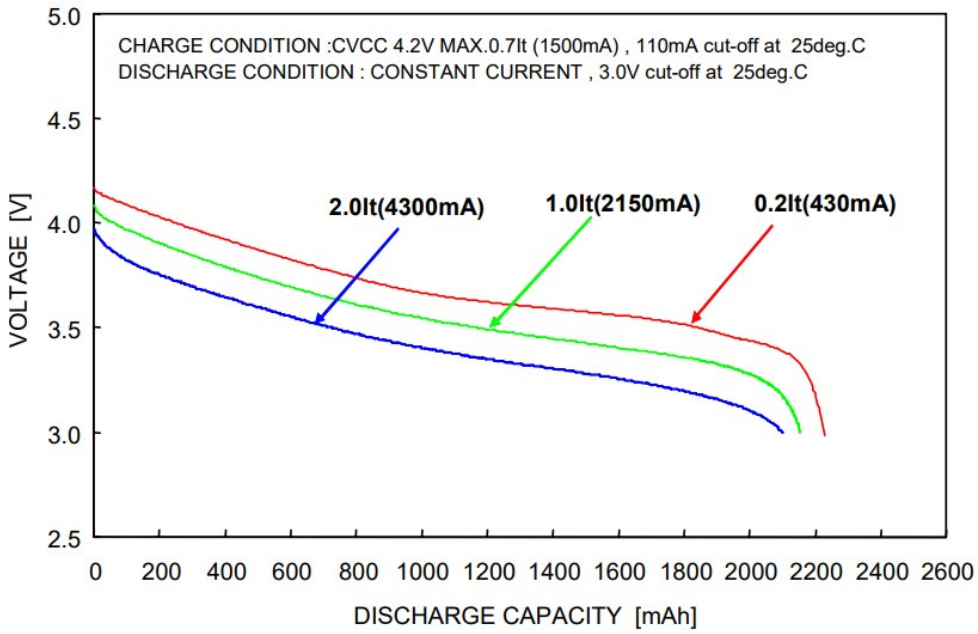

Figure 1.3: Internal resistance variation for different discharge currents and different SOC levels [17].

Temperature

Temperature has a significant impact on battery SOC measurement, higher temperatures tend to increase the state of charge, while lower temperatures have the opposite effect, This is because battery capacity and performance are temperature-dependent. At higher temperatures, the battery may experience greater self-discharge, leading to an overestimation of the state of charge, conversely, low temperatures can reduce battery performance, leading to an underestimation of service life, for example; in [9] a focused study on lithium-ion batteries and their performance at different ambient temperatures. A simplified and computationally efficient battery model was developed, requiring only a few estimated parameters for on-board application. An OCV-SOC-temperature table was integrated

into the model to improve accuracy, based on OCV tests conducted from 0°C to 50°C with a 10°C interval, SOC estimation performance was evaluated using dynamic loading tests and the unscented Kalman filtering approach, comparing the developed model to an original model that did not consider temperature, the results demonstrated that the developed battery model provided more accurate SOC values with smaller RMSE estimated errors at varying temperatures, within the SOC range of 25% to 85%. The following figure demonstrates the relationship between OCV and SOC in different temperature tests for Panasonic CGR18650CG cell [17]:

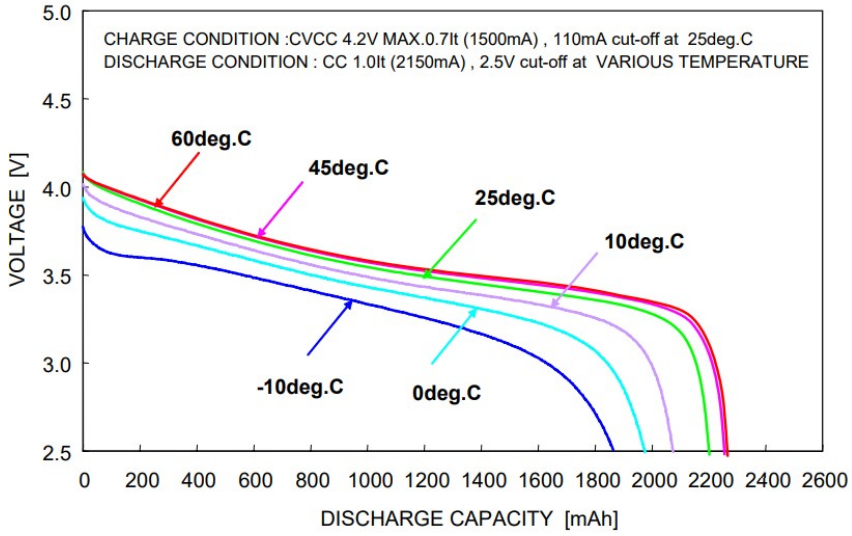

Figure 1.4: OCV–SOC curves between 30% and 80% SOC at different temperatures for Panasonic CGR18650CG [17].

1.6.2 State of Health

Over time, lithium batteries will inevitably suffer from aging and reduced capacity as a result of extended use or storage. State of health (SOH) serves as a measure of a lithium battery's current ability to hold electrical charge. As a battery ages, various performance indicators may change, including its rechargeable and discharge capacities, internal resistance, terminal voltage, cycle times, and more. To assess the SOH of a lithium battery, metrics such as battery capacity, internal resistance, and remaining cycle

count are often used [18]. Several factors can influence the lifespan of lithium batteries. Factors that can influence the lifespan of a lithium battery include [18]:

Temperature

Conventional lithium batteries operate best between temperatures of 0 to 40℃, with irreversible capacity degradation occurring outside of this range. Capacity decay rate of the battery increases with decreasing temperature. At low temperatures, lithium ion loss is the main cause of capacity loss. In contrast, at high temperatures, irreversible thermal runaway may occur, resulting in safety hazards such as spontaneous combustion and explosion due to the production of gas and heat [19].

Overcharge and Overdischarge

To prevent damage from overcharging, the Battery Management System (BMS) cuts off the power supply once the lithium battery's SOC reaches 100%. Similarly, when the battery's discharge reaches the cut-off voltage, the discharge is stopped to avoid irreversible damage caused by power loss. Overcharging causes the battery capacity to drop rapidly, leading to accelerated aging, instability, and reduced safety. Overcharge also leads to dendrite formation due to lithium ion deposition, generating heat and damaging the electrolyte solution. Over-discharging a single cell in a lithium battery pack can easily lead to a serious internal short circuit, which increases with the depth of over-discharge. Discharging the battery below the cut-off voltage and then discharging more than 20% of the SOC can cause irreversible internal short circuit damage to the battery [20].

High Current Charge and Discharge

The energy density of lithium batteries has not improved much despite their widespread use, resulting in insufficient battery life per charge, especially for portable electronic devices and long-range electric vehicles. To address this issue, charging time must be reduced. Fast charging technology, which increases total charging power by increasing

charging current, is widely used in mobile phone chargers and car charging stations. Battery aging experiments conducted in [21], found that the loss of battery capacity increases with the charging current, and the battery internal resistance also increases rapidly with the increase of charging current.

Charge–Discharge Cycle Interval

Most people tend to charge their mobile phones and electric vehicles for a longer time even after they are fully charged to ensure longer use-time. However, according to Ref[22], an aging cycle experiment was conducted on lithium batteries in four categories, Case 1(75%-65%), Case 2(75%–25%), Case 3(85%–25%), and Case 4(100%–25%), which are obtained by dividing the SOC of the battery. Therefore, it is concluded that recycling in the high SOC interval accelerates the aging of lithium batteries while recycling in the middle and low SOC interval extends the battery lifespan [21].

Charge Saturation When Shelved

Manufacturers are concerned about maintaining the best performance of lithium batteries during transportation and storage. As such, it is recommended that batteries not be put into use immediately after production. In a study cited in [23], the capacity, internal resistance, and discharge performance of batteries were tested after being placed in a thermostat with different levels of charge for three months. Results showed that batteries with either too low or too high a charge experienced greater decline in performance when stored for extended periods. It was concluded that for long-term storage, it is better to keep lithium battery charge levels at 40%-60% capacity to ensure optimal performance.

1.6.3 State of function

The State of Function (SOF) of a battery refers to its capability to fulfill a specific application's power requirements based on its current condition [11]. It is a measure used to determine whether the battery is suitable for powering the application considering its

SOC and SOH. Typically, the SOF of a battery is assessed using a digital scale, indicating whether the battery can adequately support the application or not [24]. SOF is affected by :

- State of Charge (SOC)
- State of Health (SOH)
- Maximum Delivered Power
- Temperature

1.7 Battery Management System

A "BMS" or battery management system is an on-board electronic device for monitoring and managing battery energy. Figure 1.5 shows a synoptic diagram of a BMS. There are several varieties of BMS depending on the manufacturer and the battery technology used [1]. Its main functions are:

- **Cell Balancing:** This function ensures that each individual cell within a battery pack is charged and discharged uniformly, preventing capacity imbalances and maximizing overall battery performance [25].
- **SOC Estimation:** The BMS monitors the SOC of the battery, which represents the remaining usable capacity, it is also a key factor for decision making [1].
- **SOH Estimation:** The BMS assesses the overall health and aging of the battery by monitoring parameters such as capacity fade, internal resistance, and other factors that affect the battery's performance and longevity [25].
- **Safety and Protection:** The BMS provides safety mechanisms to prevent overcharging, over-discharging, and excessive temperature conditions. It also includes features like short circuit protection and fault detection to ensure safe operation of the battery system [26].

- **Charging:** The additional function of a BMS is charging control, it oversees the charging process to ensure safe and efficient charging of the battery. It manages parameters such as charging voltage, current, and charging duration to prevent overcharging, which can lead to battery degradation or safety hazards [26]. The BMS may incorporate various charging algorithms, the most known is Constant Current Constant Voltage (CCCV) method.

The CCCV charging method described employs a current limitation during the initial charging phase to avoid over-current. It offers the benefit of straightforward determination of charging current based solely on battery capacity and charging duration. However, a notable drawback of this method is the accumulation of errors in existing SOC estimation algorithms, which can result in overcharging or undercharging, leading to a diminished battery lifespan. Consequently, this charging method is rarely adopted in modern BMSs for EVs [26].

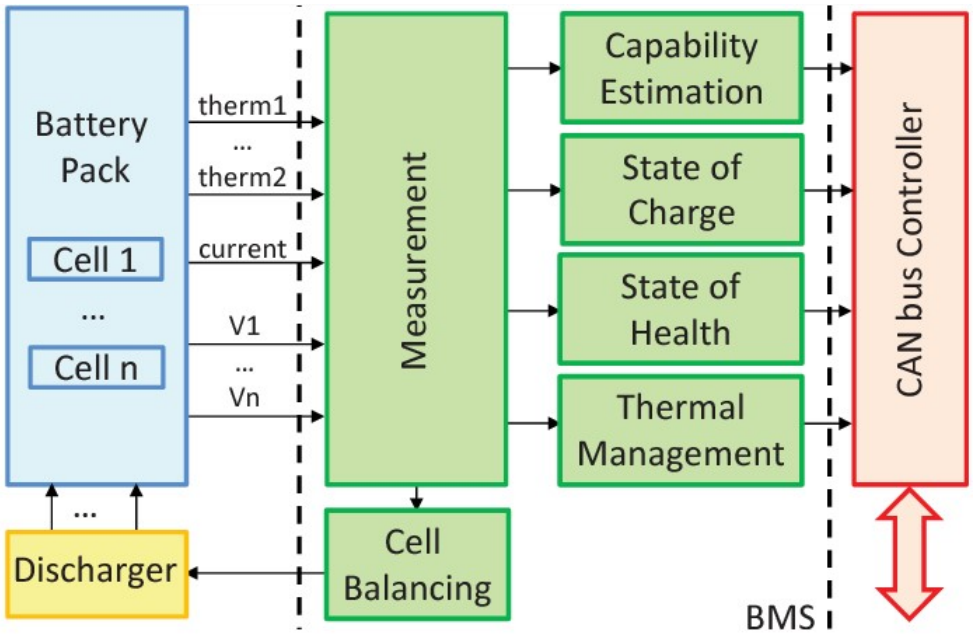

Figure 1.5: Synoptic diagram of a BMS

1.8 Conclusion

In conclusion, this chapter provided an overview of state-of-the-art battery technologies, with a focus on lithium-ion batteries. These batteries have become popular due to their high energy density, long lifespan, lightweight nature, and low self-discharge rate. They are widely used in portable electronic devices and are increasingly being adopted in electric vehicles.

The chapter also discussed the characteristics of batteries, including nominal voltage, capacity, internal resistance, life cycle, charge/discharge rate, and operating temperature. These characteristics are essential in determining the performance and lifespan of a battery.

A comparison was made between lithium-ion batteries and other conventional battery types such as lead-acid, nickel-cadmium, and nickel-metal hydride batteries. Lithium-ion batteries were found to outperform other types in terms of energy efficiency, power density, compact design, wide temperature range, fast charging, long cycle life, low self-discharge, and high efficiency in energy, charge, and voltage.

Furthermore, the chapter explored different types of lithium-ion cells, including LCO, LMO, NMC, LFP, NCA, LTO. Each type has its own advantages and disadvantages, making them suitable for different applications.

The SOC of a battery is determined by the ratio of the discharged charge to its rated capacity. SOC measurement is influenced by various factors, including the open circuit voltage, discharge current, and temperature.

In summary, highlighting the importance of SOC in batteries emphasizes the need for accurate SOC estimation for efficient control strategies, energy conservation, and battery lifespan enhancement. Additionally, considering factors such as OCV, discharge current, temperature, and SOH is crucial for reliable battery management and optimal performance. Battery management systems play a key role in monitoring and managing battery energy to ensure safe and efficient operation.

Chapter 2

Advanced SOC Estimation Techniques: From Traditional Methods to FNN Adaptation

2.1 SOC Estimation Methods

Accurate SOC estimation is important for several reasons. Firstly, it enables users to effectively monitor and manage the available energy, allowing them to make informed decisions regarding energy consumption and usage patterns. For example, in electric vehicles, accurate SOC estimation helps drivers plan their journeys and avoid unexpected battery depletion [15].

Additionally, precise SOC estimation is vital for ensuring reliable and safe operation of battery systems. It helps prevent overcharging, which can shorten battery life, and undercharging, which can lead to premature shutdowns. By accurately estimating SOC, battery management systems can implement appropriate charging and discharging strategies, maximizing the performance and overall lifespan of the battery [1].

Moreover, SOC estimation is valuable for optimizing battery usage and efficiency. By

having an accurate understanding of the remaining energy, it becomes possible to implement intelligent energy management strategies, to maximize the overall energy utilization and efficiency of battery systems.

2.1.1 Methods Based on Direct Measurement

The direct measurement approach pertains to the evaluation of distinctive physical attributes of a battery, which encompass terminal voltage and impedance. Diverse strategies have been adopted for direct measurement, like the open circuit voltage, terminal voltage, impedance quantification, and impedance spectroscopy, as documented in [15].

Open Circuit Voltage Method

The OCV method is a direct measurement technique used to estimate the SOC of a battery by analyzing its OCV. The SOC is determined by referencing the OCV of the battery, as shown in Figure 1. However, it's important to acknowledge that the OCV-SOC relationship can vary across different battery types, and the conventional OCV-SOC model may not be universally applicable [27]. While the OCV method offers accurate SOC estimation, it does have certain limitations.

One limitation of the OCV method is that it requires disconnecting the battery from the load for a minimum of two hours to obtain reliable voltage measurements. However, this prolonged disconnection time may not be practical or feasible for many battery applications. As a result, the OCV method may not be suitable for scenarios that require frequent and immediate SOC estimation [7].

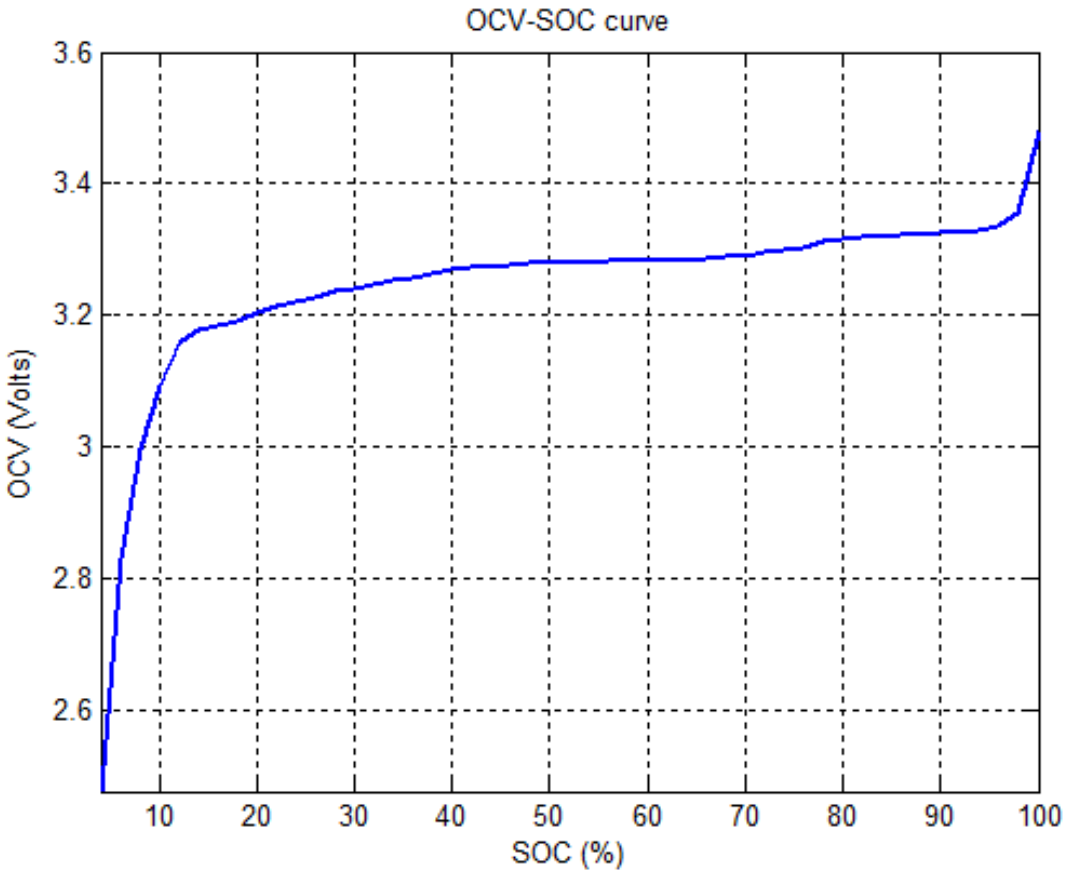

Figure 2.1: Experimental OCV-SOC curve for LFP cell [28].

Terminal Voltage Method

The Terminal Voltage Method is a SOC estimation technique that relies on the relationship between the voltage drops at the battery terminals and the internal impedance during discharge. The electromotive force of the battery is directly proportional to the terminal voltage. This method has been tested across different discharge currents and temperatures to establish its effectiveness. However, it is important to consider that the accuracy of the terminal voltage method can be influenced by the internal resistances of the battery, which may vary with usage and aging. Consequently, this method may not always yield precise SOC estimates [29].

Impedance Spectroscopy Method

Impedance measurements have the potential to provide insights into a battery's SOC. However, different batteries exhibit distinct impedance parameters and their variations with SOC. Thus, conducting a comprehensive set of impedance experiments becomes necessary to identify and utilize these parameters for SOC estimation. In order to estimate the SOC using impedance measurements, the model impedance values can be determined by fitting the measured impedance values to the known impedance values at different SOC levels. This approach enables the estimation of SOC based on the impedance characteristics of the battery [30].

2.1.2 Book-keeping Method

The book-keeping estimation method uses the battery's discharging current data as input. This method considers some internal battery effects such as self-discharge, capacity-loss, and discharging efficiency. Two types of book-keeping estimation methods are used: Coulomb counting method and modified Coulomb counting method.

Coulomb Counting Method

Coulomb counting is a widely used method for estimating SOC. This method is based on the principle that the amount of charge flowing into or out of a battery is equal to the product of the current and time [31]. By measuring the current and integrating it over time, the accumulated charge entering or leaving the battery can be calculated. The SOC can then be estimated using the following equation:

$$SOC(t) = SOC(t-1) + \frac{\int_{t-\Delta}^{t} I(\tau)d\tau}{Qn} \tag{2.1}$$

In this equation, $SOC(t)$ represents the state of charge at time t, $SOC(t-1)$ is the state of charge at the previous time step, $I(t)$ denotes the current at time t, Q is the battery capacity, n represents the number of series-connected cells, and Δ is the sampling time interval.

The accuracy of the coulomb counting method depends on the precision of the initial SOC estimate and the accuracy of battery current measurement, which is influenced by the accuracy of current sensors. This method may accumulate errors over time and is not ideal for real-time SOC estimation. However, it can be employed to validate the precision of SOC estimations generated by other methods [32].

The modified Coulomb counting method is a variation of the Coulomb counting method that considers the non-linear relationship between the battery's voltage and SOC. This approach incorporates a correction factor based on the battery's voltage to refine the SOC estimate, leading to improved accuracy [31].

2.1.3 Methods Based on Adaptive Systems

Adaptive systems represent a category of SOC estimation methods specifically designed for lithium-ion batteries. These systems possess the capability to autonomously design and adjust the SOC estimation algorithm to accommodate various discharging conditions. Over the past few years, several novel adaptive systems for SOC estimation have emerged, including:

Feed Forward Neural Network

FNN is a type of ANN widely utilized for SOC estimation due to its ability to handle complex and nonlinear relationships between input and target variables. This network consists of an input layer that takes in current, voltage, and temperature values, one or more hidden layers for nonlinear mapping, and an output layer for estimating SOC. The nodes within the layers are interconnected, and activation functions are employed in the hidden and output layers to add nonlinear relationship [28]. The architecture of a feed-forward neural network for SOC estimation is depicted in Figure 2.2.

The output y_j of a processing node j in either the hidden or output layer is determined by the following equation:

$$y_j = F(u_j) = F\left(\sum_i x_{ij} w_{ji} + b_j\right) \tag{2.2}$$

In this equation, y_j represents the output of node j, F denotes the activation function, u_j is the weighted sum of inputs to node j, x_{ij} refers to the input from node i to node j, w_{ji} represents the weight associated with the connection between nodes i and j, and b_j signifies the bias term for node j.

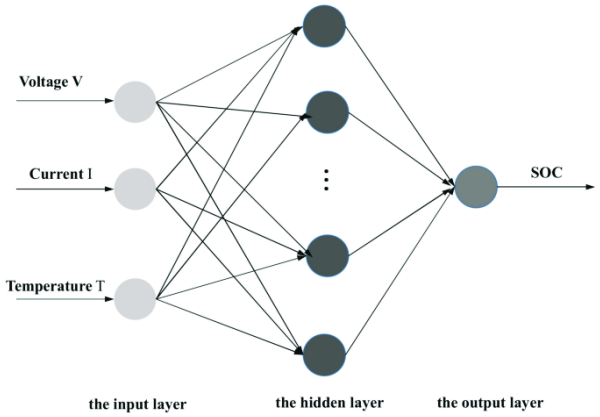

Figure 2.2: The architecture of the SOC estimating FNN [28].

RBF Neural Network

The Radial Basis Function (RBF) neural network is widely employed for SOC estimation in batteries due to its nonlinear mapping capabilities, self-organizing learning ability, fast training, and ability to converge to global optimization, resulting in optimal function approximation. The structure of an RBF neural network consists of an input layer, a hidden layer, and an output layer [33].

The output $h_j(X)$ of the j^{th} neuron in the hidden layer is computed as follows:

$$h_j(X) = \varphi(|X - C_j|), \tag{2.3}$$

Here, $\varphi(\cdot)$ represents the radial basis function, $C_j \in R^n$ denotes the center of the j^{th} hidden neuron, and $|\cdot|$ represents the Euclidean norm [33].

The SOC estimation output $Y(X)$ is obtained by linearly combining the signals from the hidden layer's outputs $h_j(X)$ using synaptic weights:

$$Y(X) = \sum_{j=1}^{m} w_j h_j(X), \tag{2.4}$$

where w_j represents the synaptic weight associated with the j^{th} neuron in the hidden layer.

If the Gaussian function is chosen as the radial basis function $\varphi(\cdot)$, the expression for $h_j(X)$ is given by [33]:

$$h_j(X) = \exp\left(-\frac{|X - C_j|^2}{2\sigma_j^2}\right), \tag{2.5}$$

Here, σ_j represents the spread of the j^{th} neuron for the input signal.

Support Vector Machine

Support Vector Machines (SVM) are powerful supervised learning methods used for both classification and regression tasks. They possess the capability to approximate multivariate functions with high accuracy. Initially developed for solving classification problems, SVM models are built based on a subset of the training data. This is achieved by utilizing a cost function that disregards points beyond the margin and training data that are close (within a threshold) to the model prediction [34]. As a result, SVM can effectively generalize and make accurate predictions.

Kalman filter

this method uses lithium cell Equivalent Circuit Model (ECM), which aim to reproduce the behaviour of the electrical quantities in the battery (SOC, Voltage and current) and allows them to be easily formulated into mathematical formula. This model, as shown in Figure 2.3, use standard electrical components such as resistors, capacitors and voltage source. The values of the model are obtained from experimentation [1]. This Step Allow

us better understanding and simulating the behaviour of lithium cell, however The ECM in Simulink has limitations including oversimplification, parameter variability, limited dynamic response, model complexity, aging effects, and varying validity across battery chemistries.

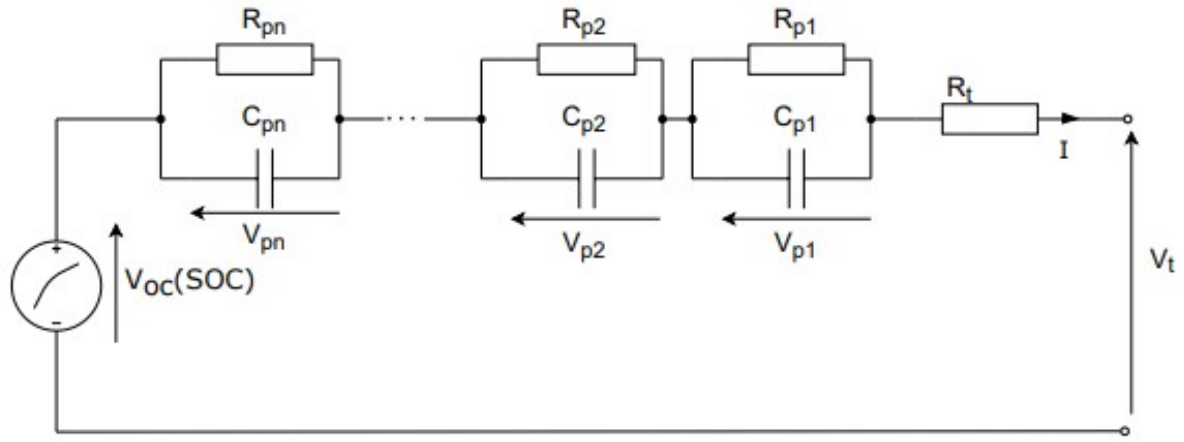

Figure 2.3: RC complex ECM for lithium cell [1]

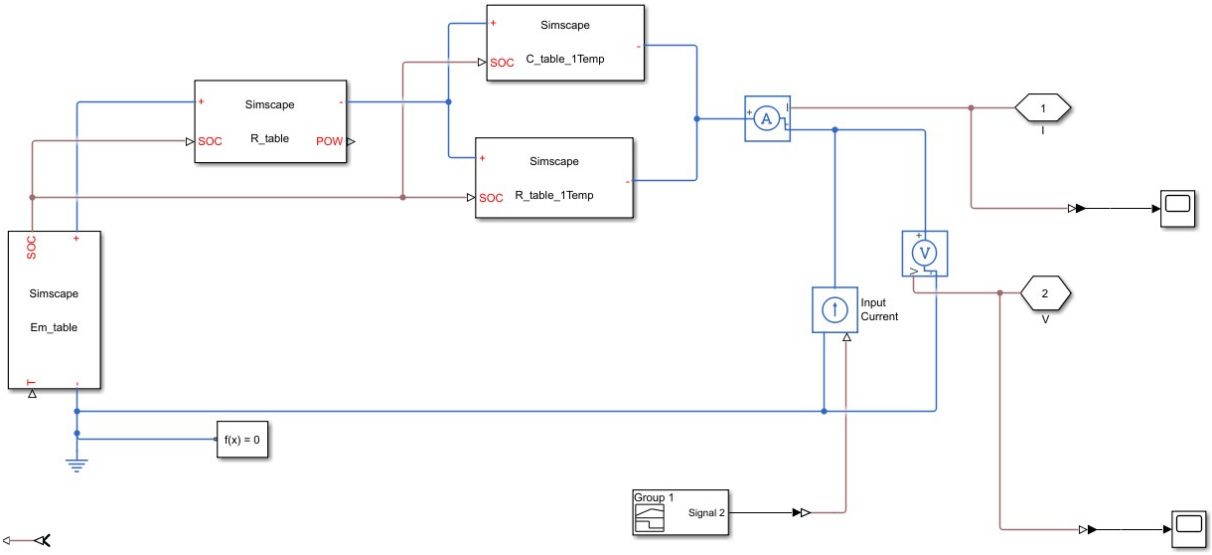

Figure 2.4: RC complex equivalent electrical model in MATLAB Simulink

The state equation describing this electrical system is given as follow [1]:

$$
\begin{cases}
\begin{bmatrix} \dot{SOC} \\ \dot{V_{p1}} \\ \dot{V_{p2}} \\ \vdots \\ \dot{V_{pn}} \end{bmatrix} = \begin{bmatrix} 0 & 0 & 0 & \cdots & 0 \\ 0 & \frac{-1}{R_{p1}C_{p1}} & 0 & \cdots & 0 \\ 0 & 0 & \frac{-1}{R_{p2}C_{p2}} & \cdots & 0 \\ \vdots & \vdots & \vdots & \ddots & \vdots \\ 0 & 0 & 0 & \cdots & \frac{-1}{R_{pn}C_{pn}} \end{bmatrix} \cdot \begin{bmatrix} SOC \\ V_{p1} \\ V_{p2} \\ \vdots \\ V_{pn} \end{bmatrix} + \begin{bmatrix} \frac{1}{C_{actual}} \\ \frac{1}{C_{p1}} \\ \frac{1}{C_{p2}} \\ \vdots \\ \frac{1}{C_{pn}} \end{bmatrix} \cdot I \\
V_t = \begin{bmatrix} a & 1 & 1 & \cdots & 1 \end{bmatrix} \cdot \begin{bmatrix} SOC \\ V_{p1} \\ V_{p2} \\ \vdots \\ V_{pn} \end{bmatrix} + R_t \cdot I + b
\end{cases}
\tag{2.6}
$$

The system dynamics are first translated into a model, which is then used in conjunction with a Sliding Mode Observer to estimate the state of charge. However, the estimated SOC is subject to noise, so a Kalman filter is employed to remove the noise and improve the accuracy of the SOC estimation [1].

2.1.4 Hybrid Methods

Hybrid methods for SOC estimation of lithium batteries leverage the strengths of multiple SOC estimation techniques to enhance accuracy and performance. By integrating various methods, such as Coulomb counting, Kalman filter, and neural networks, hybrid models can effectively address the limitations and uncertainties associated with individual methods.

Research studies have demonstrated that hybrid methods generally yield more accurate SOC estimations compared to single methods. However, developing a hybrid model necessitates careful selection and optimization of each method, along with determining suitable weighting and fusion strategies for combining the results [15].

2.2 Adopted Method: Feed Forward Neural Network

This section focuses on elaborating FNN model for SOC estimation. The chapter introduces the objectives and approach of the study, followed by a description of the experimental setup. It discusses data acquisition, cell specifications, and the dataset used for the study.

Explaining the data selection and normalization techniques used, including the application of the Min-Max normalization algorithm and a moving average filter. It then delves into training FNN model. Adjusting parameters and Hyper-parameters is described.

The results of the training process are analyzed through regression, performance and gradient plots. Comparison graphs between the actual and predicted values demonstrate the accuracy of the model, highlighting its architecture and performance.

2.2.1 Experimental Procedure: Supervised BP Learning

- Selection of the input and the output data for the supervised BP learning.
- Normalization of the input and the output data.
- Training of the normalized data using BP learning.
- Testing the goodness of fit of the model.
- Comparing the predicted output with the desired output.

Figure 2.5 illustrates a flowchart summarizing the process for developing an accurate SOC estimation model.

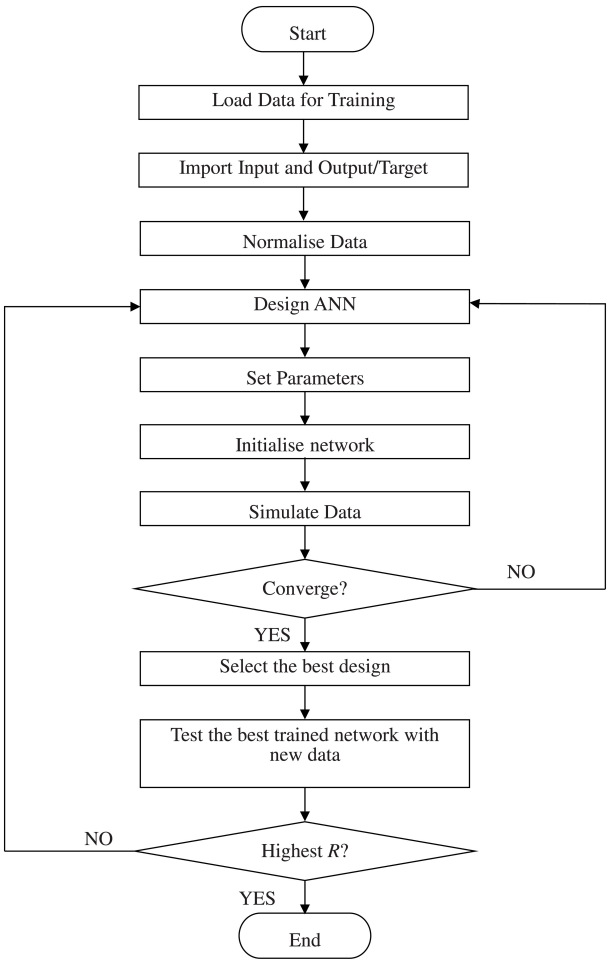

Figure 2.5: Experimental Procedure

2.2.2 Dataset Selection and Data Preprocessing

The dataset used in this study is sourced from [18], specifically collected using the 'Digatron Firing Circuits Universal Battery Tester channel', known for its high accuracy. Due to hardware limitations, focusing on the dataset 25°C, assuming ambient temperature conditions. Table 2.1 provides an overview of the essential data information.

Table 2.1: Data Information

Lithium Cell Name	LG HG2
Capacity	3000 mAh
Selected Inputs	Voltage, Current, Temperature
Training Data	Mixed (1-8)
Validation Data	20% of Training Data
Testing Data	Drive cycles
Normalization Function	Min-Max
Software Used	MATLAB, Python

Min Max Normalization

Min-max normalization is a commonly used data preprocessing technique that scales the values of a dataset to a fixed range, typically between 0 and 1. It is useful when the range of values across different features of a dataset is significantly different, as it can improve the performance of machine learning models by reducing the impact of outliers and ensuring that all features are on the same scale. Additionally, it can help with faster convergence during training and avoid issues caused by numerical instability [35].

Moving Average Filter

In signal processing, the use of a moving average filter (MAF) is a common technique to mitigate noise and remove undesired fluctuations from a signal. This technique involves computing the mean value of a small segment of consecutive data points within the signal and substituting each data point with the computed mean value. This process is repeated iteratively for all the data points, leading to a smoothed signal with reduced noise [36].

$$\text{min-max normalization}(x_i) = \frac{x_i - \min(x)}{\max(x) - \min(x)}$$

Figure 2.6displays a plot of the training data.

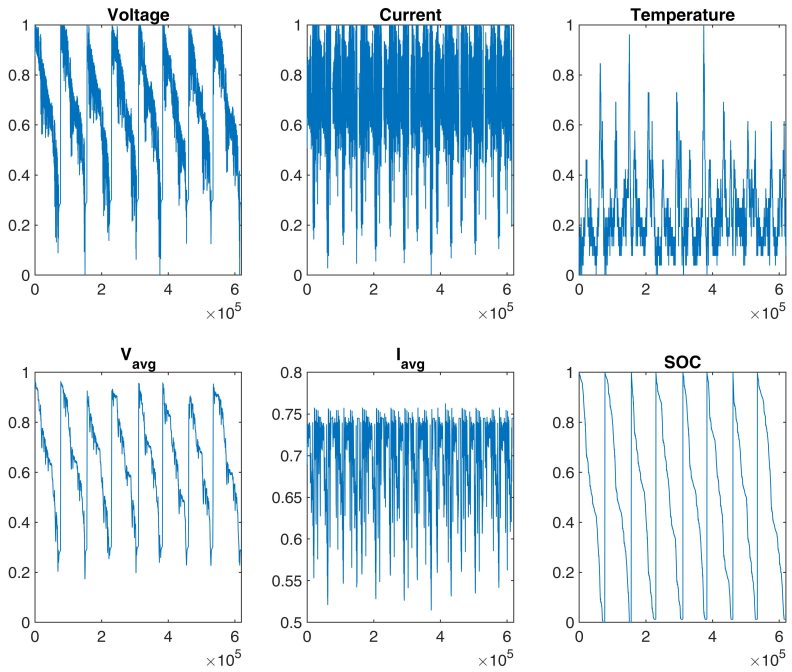

Figure 2.6: Training data plot

2.2.3 Neural Network Model Training

Using "nntool" – open network/data manager in Matlab, network properties are shown in the following table :

Table 2.2: FNN model properties

Neural Network Properties	
Network Type	Feedforward Backprop
Training Function	Levenberg-Marquardt (trainlm)
Adaption Learning Function	LearnGDM
Performance Function	MSE
Activation Function	Tansig
Number of Epochs	30
Number of Hidden Layers	2
Number of Neurons	40×7

In the Neural Fitting Tool of MATLAB "NFTOOL", the regression curve is a graphical

representation of the fit between the actual and predicted values of the output variable. It is a plot of the predicted values against the actual values, where the ideal curve is a straight line that passes through the origin with a slope of 1. The regression is plotted in Figure 2.7.

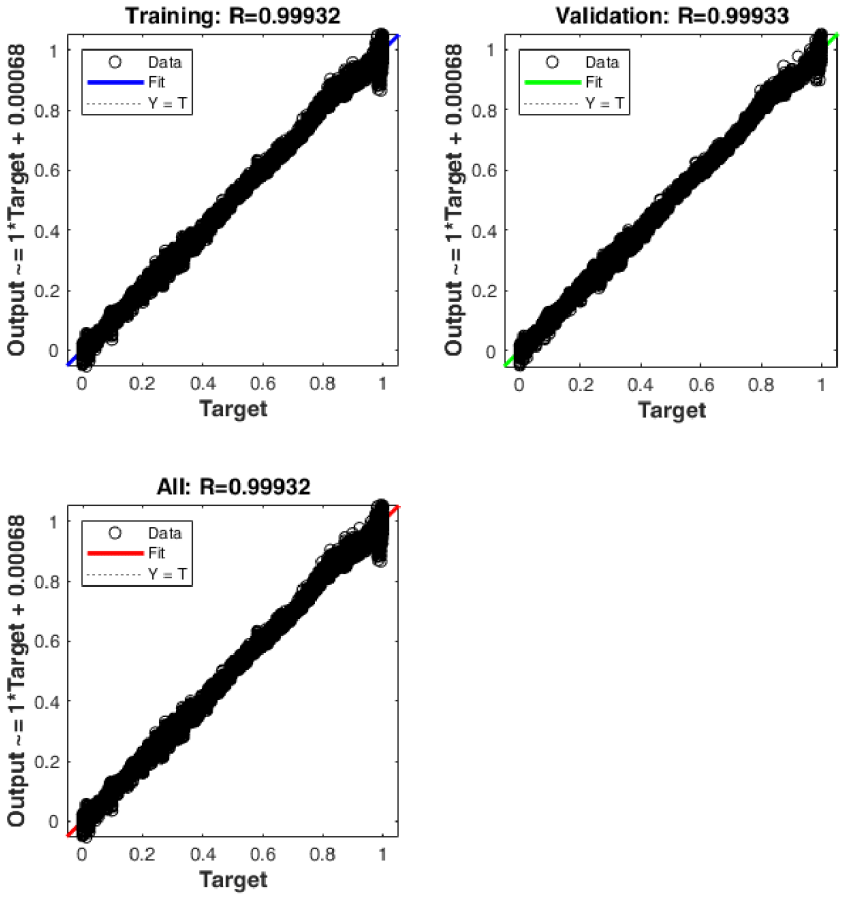

Figure 2.7: Regression Plot

The gradient plot is a visual representation of the magnitude of the gradients of the weights with respect to the error function during the training process. The plot shows the average gradient magnitude for each layer of the network as a function of training time or epoch. The gradient plot is useful for monitoring the progress of training and diagnosing potential issues, such as slow convergence or oscillations in the weights.

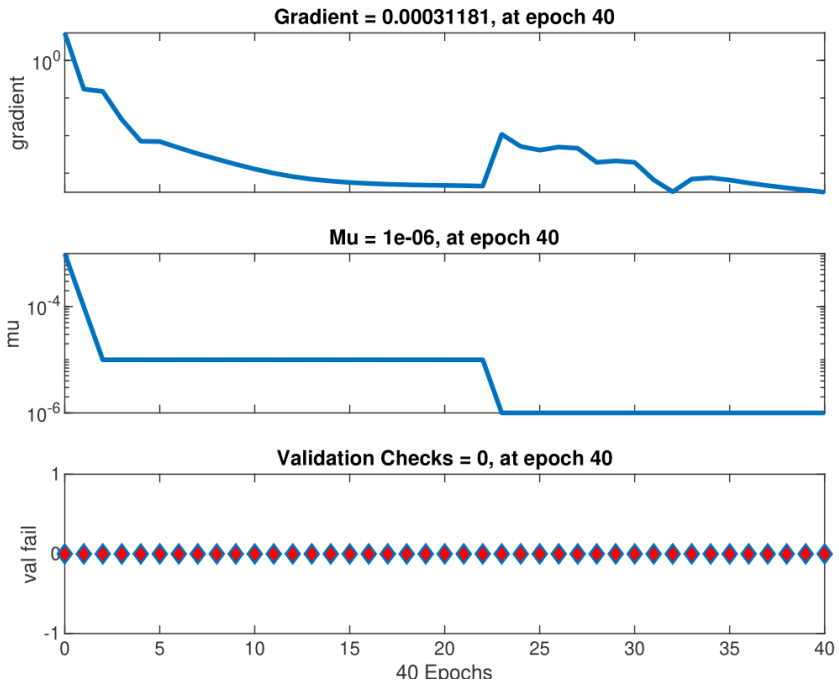

Figure 2.8: Training State

Upon analyzing 2.8, it can be observed a steady decrease in the plot, indicating that the weights are adjusting significantly to improve the training's fit. However, at epoch 22, there was a rise in the gradient plot due to the decrease in the learning rate.

Figure 2.9 represents a comparison graph between the actual SOC and the predicted SOC of the testing data.

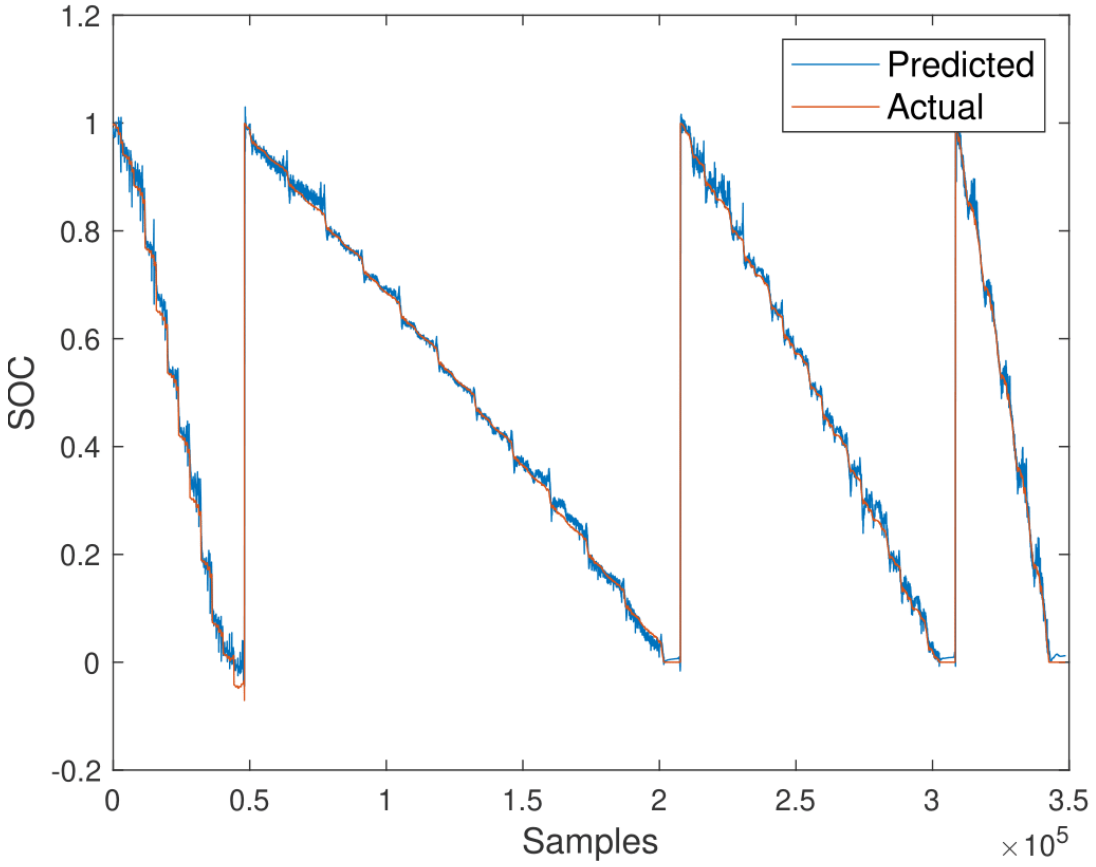

Figure 2.9: Estimated Values vs real values

Based on 2.9, a fairly good results with a high degree of accuracy has been obtained, as indicated by the MAE value of 0.0095. However, the graph also shows some noise that can be reduced by applying a MAF.

2.2.4 Noise Elimination Using Moving Average Filter

After examining the earlier findings, it is observed that the curve representing the predicted values of SOC exhibits noise. To address this issue, a potential solution involves implementing MAF to mitigate the impact of minor SOC fluctuations during the discharge process of the lithium cell, as facilitated by the battery management system. Figure 2.10 illustrates the filtered predicted values for 2.9 and 2.11 shows the error between filtered and original SOC, showcasing the effectiveness of this approach in reducing noise.

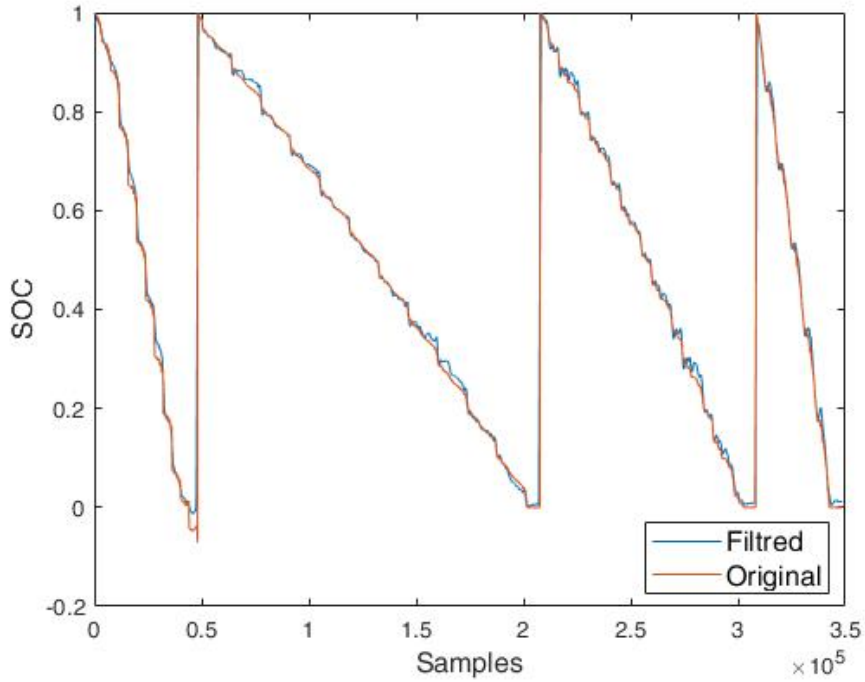

Figure 2.10: Filtered values using MAF

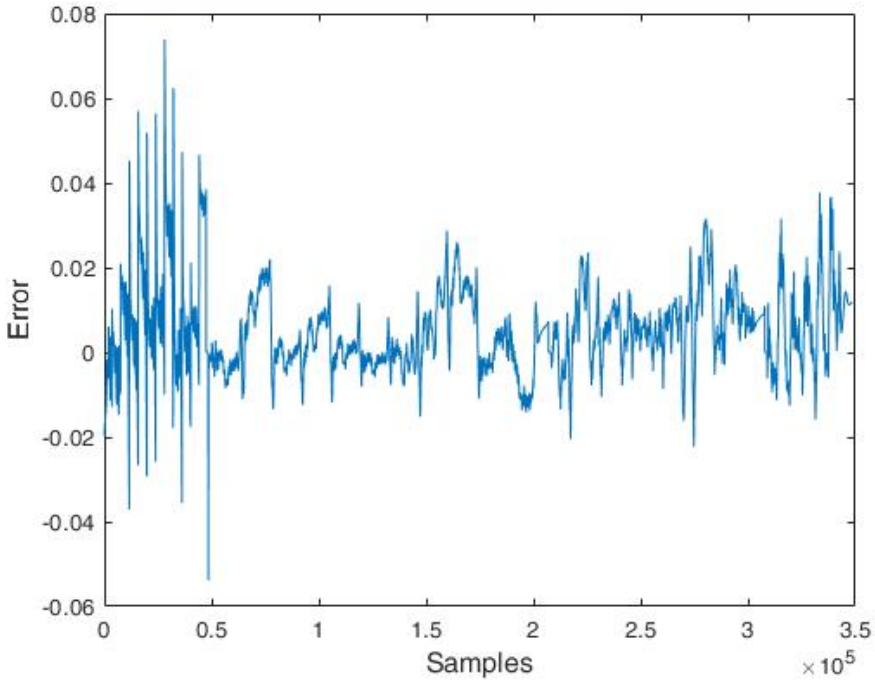

Figure 2.11: Error between Filtered SOC values and actual SOC

2.3 Conclusion

In conclusion, this chapter discussed advanced SOC estimation techniques, starting from traditional methods and leading to the adaptation of FNN. Accurate SOC estimation is important for effective energy management, reliable battery operation, and optimizing battery usage and efficiency.

The chapter first highlighted the importance of accurate SOC estimation, emphasizing its role in monitoring energy levels, making informed decisions about energy consumption, and ensuring the longevity and performance of battery systems.

Next, exploring direct measurement methods for SOC estimation, including the OCV method, terminal voltage method, and impedance spectroscopy method. Each method was discussed in terms of its principles, advantages, and limitations.

The book-keeping method, specifically the Coulomb counting method, was also explained as a widely used technique for SOC estimation. The principle of Coulomb counting, its equation for SOC estimation, and its limitations were discussed. The modified Coulomb counting method, which addresses the non-linear relationship between voltage and SOC, was also mentioned.

The chapter then introduced adaptive systems for SOC estimation, with a focus on the FNN model. The architecture of the FNN model was described, highlighting its input layer, hidden layers, and output layer. The equations for calculating the output of each node in the FNN model were presented.

The chapter concluded with a detailed exploration of the FNN model for SOC estimation. The experimental procedure for supervised BP learning was explained, including the selection and normalization of input and output data. The training process, parameter adjustment, and hyper-parameter optimization were also discussed. The results of the training process, including regression analysis, performance evaluation, and comparison between actual and predicted values, demonstrated the accuracy and performance of the FNN model.

Chapter 3

Design and Implementation

3.1 Introduction

The implementation and realization phase is a critical step in any project design, as it involves the actual construction of the conceptual model developed earlier. This phase serves to validate the conceptual model and to identify any previously undiscovered issues. In the next chapter, it will be discussed about the various software, development, and programming tools used to build our prototype.

3.2 Programming Language

The source code governing the Arduino Mega microcontroller is written in the C language. Arduino is a widely used microcontroller platform that is popular among hobbyists and professionals alike for a wide variety of applications. The C language is a natural choice for the development of embedded systems on the Arduino Mega, appreciated for its efficiency and ability to interact with hardware [37].

Originally designed in the 1970s to write the first versions of the Unix operating system, C has become one of the most widely used programming languages for developing programs that need to be fast or interact with hardware. The language was specifically designed to be close to the processor and easily compiled, enabling it to be translated into machine

language while maintaining high performance [37].

3.3 Software and Programming Tools

Various software and programming tools have been used for the implementation of this prototype, this section offers a brief description for each of them.

3.3.1 Arduino Software

Arduino Software is an integrated development environment (IDE) for programming Arduino boards. It provides an easy-to-use interface and a variety of libraries that simplify the development of embedded systems while maintaining high performance. The IDE is based on the C language, which is optimized for embedded systems and provides direct access to hardware resources [37]. Compared to other software like "Atmel Studio - Atmel Studio 7", the Arduino IDE offers a wide range of libraries (Wire Library, Servo Library...) that enable developers to save time during the development phase. With its advanced features, the Arduino IDE is a natural choice for anyone who wants to develop efficient and reliable embedded systems using Arduino boards.

3.3.2 ISIS Proteus Software

Isis Proteus is a user-friendly software designed by Labcenter Electronics to facilitate application development and simulation. Its intuitive graphical environment enables easy editing of electronic schematics and simulations. This software is beneficial during the initial stages of the project and algorithm writing as it allows for detecting errors and bugs, ultimately saving valuable time during prototype realization. ISIS Proteus have been used in order to simulate sensors with Arduino.

3.3.3 Matlab Coder

MATLAB Coder is a powerful tool that generates C and C++ code from MATLAB code. It can be used with a variety of hardware platforms, ranging from desktop systems to embedded hardware. This software supports most of the MATLAB language as well as a wide range of toolboxes. The generated code can easily be integrated into our projects as source code, static libraries, or dynamic libraries. The code produced is highly readable and portable, allowing you to combine it with critical parts of your existing C and C++ code and libraries [38].

During the experiment, a trained FNN model has been developed in MATLAB and converted into an Arduino function. By specifying the input data type and size, providing a sample for compilation, and selecting the ATmega microprocessor, an estimation function as an Arduino function has been successfully generated. The resulting Arduino code, shown in A, has a compact size of only 5 KB, which takes only 2% of memory of Arduino Mega 2560.

3.4 Electronic circuit

3.4.1 Electrical Components

Panasonic CGR18650CG Lithium Cell

The features of this cell are presented in table 3.1:

Table 3.1: Characteristics of Panasonic CGR18650CG Lithium Cell [17].

Capacity	2250m mAh
Chemistry	LCO
Operating Voltage	2.8 V - 4.2 V
Max Discharge Rate	2C

Arduino Mega 2560

Arduino Mega 2560 is a microcontroller board based on the ATmega2560. It has 54 digital input/output pins, 16 analog inputs, and four UART (hardware serial communication) ports. It also has a USB connection, which can be used to connect to a computer and program the board or monitor the data [37].

The board is designed to work with a wide range of sensors, motors, and other electrical components. It is widely used in various DIY projects, robotics, and automation. Due to its high processing power, it can handle complex tasks and run multiple programs simultaneously by using multitasking. Table 3.2 resumes the characteristics of Arduino 2560 [37].

Characteristics	**Specifications**
Microcontroller	ATmega2560
Operating voltage	5V
Digital I/O pins	54 (of which 14 provide PWM output)
Analog input pins	16
DC current per I/O pin	20 mA
DC current for 3.3V pin	50 mA
DC current for 5V pin	200 mA
Flash memory	256 KB (8 KB used by bootloader)
SRAM	8 KB
EEPROM	4 KB
Clock speed	16 MHz

Table 3.2: Characteristics of Arduino Mega2560

ACS712 Current Sensor Module

ACS712 is a current sensor module that can measure both AC and DC currents. It uses a Hall effect sensor to measure the magnetic field created by the current passing through a conductor with 185 mV/A output sensitivity. The module has a programmable output voltage, which can be set to either 5V to be compatible with Arduino or 3.3V for ESP32. It also has a built-in amplifier to amplify the signal generated by the Hall effect sensor and provide a more accurate measurement of the current [39].

MP1584EN 12V Voltage Regulator

The MP1584 is a switching regulator that steps down voltage at a high frequency. It has an internal high voltage power MOSFET on the high side. The regulator has a 3A output and uses current mode control for quick loop response and uncomplicated compensation. With an input range of 4.5V to 28V, it accommodates various step-down applications, including in automotive environments. An operational quiescent current of 100µA makes it suitable for battery-powered devices. Scaling down the switching frequency during light load conditions reduces switching and gate driving losses, resulting in high power efficiency [40].

HX1314G 5V Voltage Regulator

This is a synchronous buck regulator module based on the HX1314G chip for high voltage input. It operates within a 5.5V to 32V DC input voltage range and achieves a continuous output current of 1A with excellent load and line regulation. It also offers high conversion efficiency and low heat generation. The switching frequency is programmable from 130kHz to 500kHz and the synchronous architecture allows for highly efficient designs. Its current mode operation provides a fast transient response and facilitates loop stabilization. Its functioning principle is similar to the old LM7805 regulator but with higher efficiency and a better input range and can be directly replaced [41].

TP4056 Lithium cell charger module

TP4056 is a CCCV charger for single lithium cell, ideal for portable applications due to its small size and compatibility with USB and wall adapters. It doesn't need a blocking diode and has thermal feedback to prevent overheating. Charge voltage is 4.2v, current can be set with a resistor and it automatically stops when finished. Other features include current monitor, under voltage lockout, automatic recharge and status pins [42], Image 3.1 displays CCCV curves for this charger.

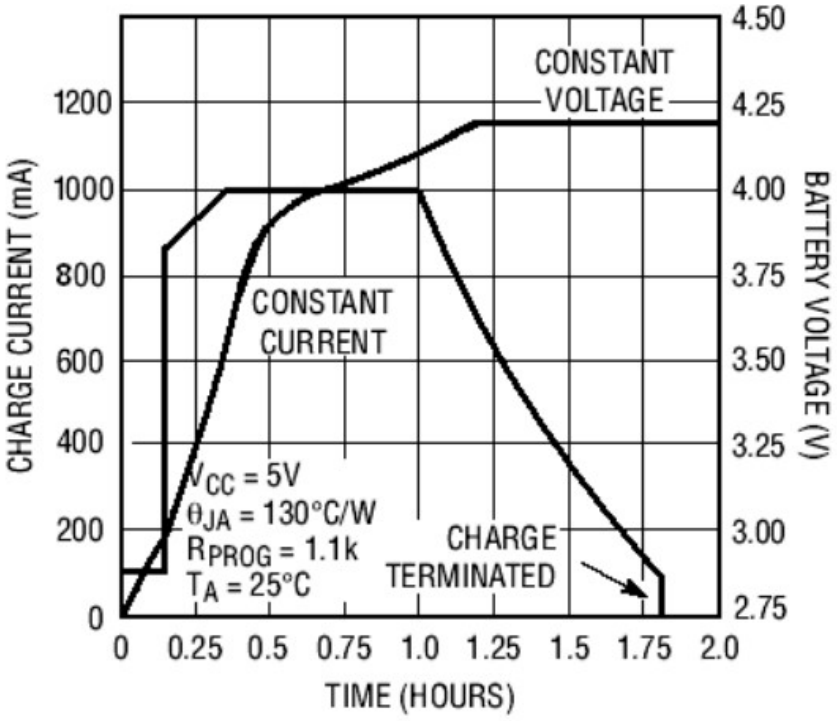

Figure 3.1: CCCV charging curve for TP4056 [42]

.

Voltage Divider (Voltage Measurement)

A voltage divider circuit employing resistors of $7.5k\Omega$ and $30k\Omega$ has been created. The circuit diagram for the voltage divider is displayed in Figure 3.2, and the value is determined using the following calculation:

$$\text{Vin} = \text{Vout} \times \left(\frac{\text{R2}}{\text{R1} + \text{R2}} \right)$$

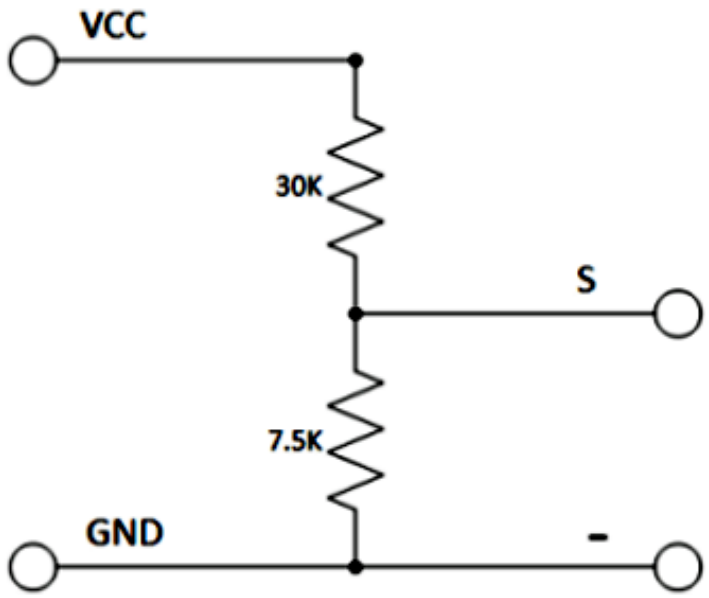

Figure 3.2: Voltage Measurement Circuit

.

3.4.2 Circuit on Breadboard

The test plate used in the experiment is a plastic plate with multiple holes. These holes are spaced 2.54 mm apart, which aligns with the standard spacing of electronic components commonly used in our assemblies. This design allows for easy testing without the need for soldering, enabling adjustments and corrections during the design and sizing phase.

To collect automatic discharge data, a circuit is employed that measures the voltage and current of each cell (connected in series). The Arduino utilizes these inputs to perform coulomb counting and normalize the values, enabling SOC calculation using the neural network function generated by MATLAB Coder. The 12V voltage regulator is responsible for establishing the output voltage and powering the Arduino. Additionally, the 5V voltage regulator supplies power to the ACS712 current sensor and any other shields that may be added to the circuit. A USB connection is necessary for serial data transfer to a computer, where the data can be visualized using MATLAB. Figure 3.3 illustrates the circuit implemented on the bread board.

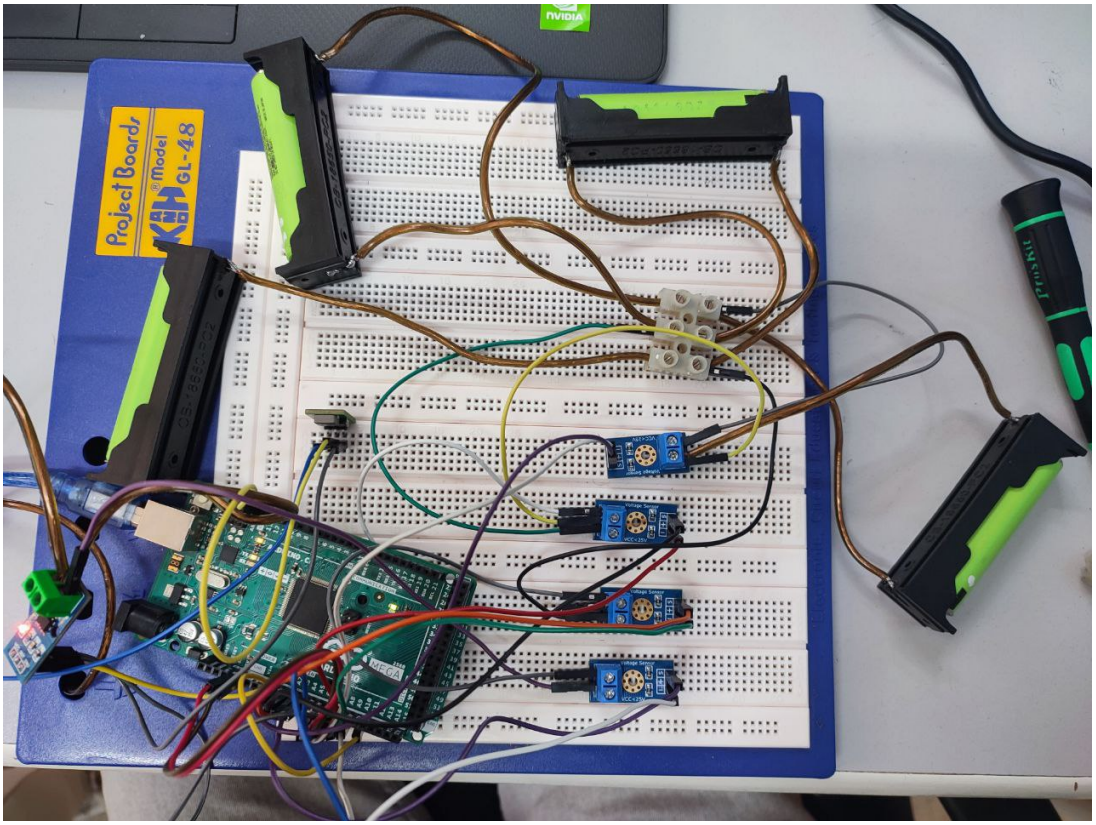

Figure 3.3: Discharge Test Circuit

.

3.5 Conclusion

In this chapter, the design and implementation of our project were discussed. The implementation phase, which involves the construction of the earlier developed conceptual model and the validation of its functionality, was addressed. The programming language used, C, was highlighted for its efficiency and hardware interaction capabilities, making it well-suited for embedded systems like Arduino.

It was also introduced the software and programming tools utilized in the implementation process. The Arduino Software, an integrated development environment, offers a user-friendly interface and libraries that simplify embedded system development. ISIS

Proteus Software was employed for simulating sensors with Arduino, aiding in error detection and saving time during the prototype phase. Additionally, MATLAB Coder was used to convert a trained FNN model into an Arduino function, generating highly readable and portable code.

The electronic circuit section provided an overview of the electrical components used, including the Panasonic CGR18650CG Lithium Cell, Arduino Mega 2560, ACS712 Current Sensor Module, MP1584EN 12V Voltage Regulator, HX1314G 5V Voltage Regulator, and TP4056 Lithium Cell Charger Module. The circuit was implemented on a breadboard, allowing for easy testing and modifications during the design phase.

Overall, this chapter presented the design and implementation details of our project, including the programming language, software tools, and electronic circuit. These elements form the foundation for the successful realization of our prototype.

Chapter 4

Implementation and Results

4.1 Introduction

In this chapter, the efforts were focused on implementing an SOC estimator model for a specific lithium cell, which is LG HG2. However, due to its unavailability in the market, a significant challenge was faced in obtaining data for training and testing our model. Consequently, Panasonic CGR18650CG was utilized as a substitute for LG HG2 in our experimental setup. By leveraging the power of AI and incorporating advanced algorithms, the aim was to explore the feasibility of training a model on LG HG2 to accurately estimate the SOC of CGR18650CG. Several intriguing questions and considerations are raised by this approach, such as the impact of cell variations on the overall model performance and its implications for real-world implementation. The limitations posed by the unavailability of LG HG2 were addressed and insights into the potential implications of utilizing CGR18650CG as a surrogate for SOC estimation. While the emphasis is on the methodology and the challenges faced, the focus is on highlighting the significance of the problem. Valuable insights to the field of battery management systems are anticipated to be contributed by our findings, aiding in the development of accurate SOC estimation techniques for future lithium cell applications.

4.2 LG HG2 cell Model

4.2.1 Results

According to the findings presented in Chapter 2, the prediction function B was integrated into the Arduino code mentioned in A. By doing so, an impressive accuracy rate of 99% was achieved. The collected results were then transmitted to MATLAB via serial reading port. Figure 4.1 illustrates the data obtained from a comprehensive test conducted to evaluate the performance, displaying the voltage of four cells along with the corresponding current flowing through them.

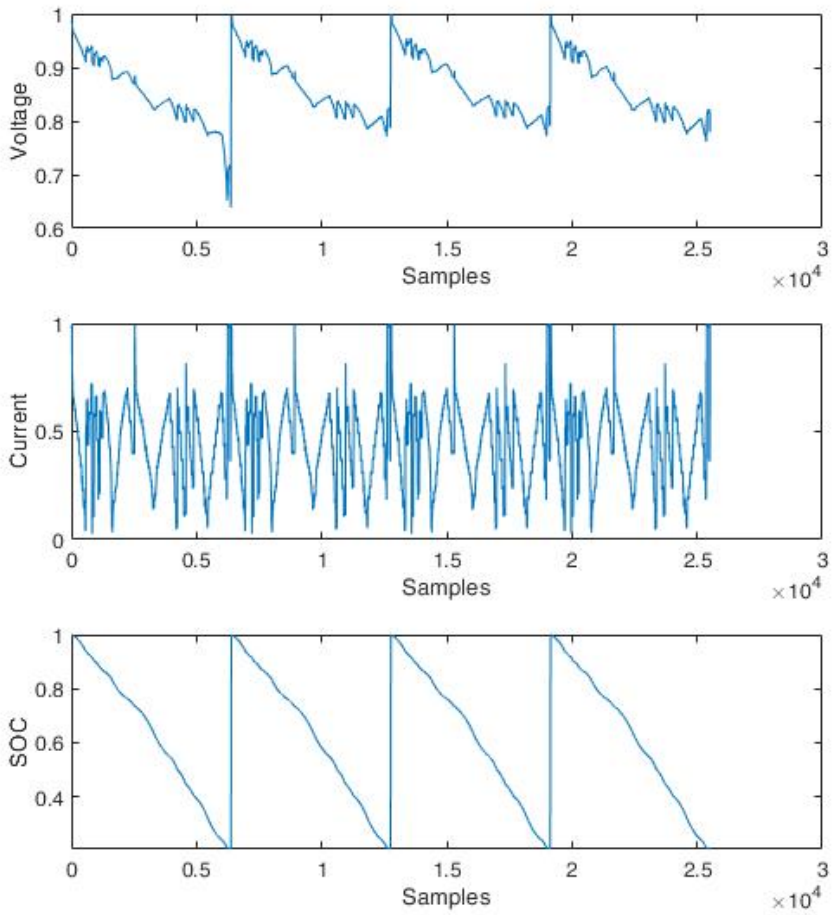

Figure 4.1: CGR18650CG testing data

Figure 4.2 shows the predicted SOC comparing to SOC calculated by Coulomb counting.

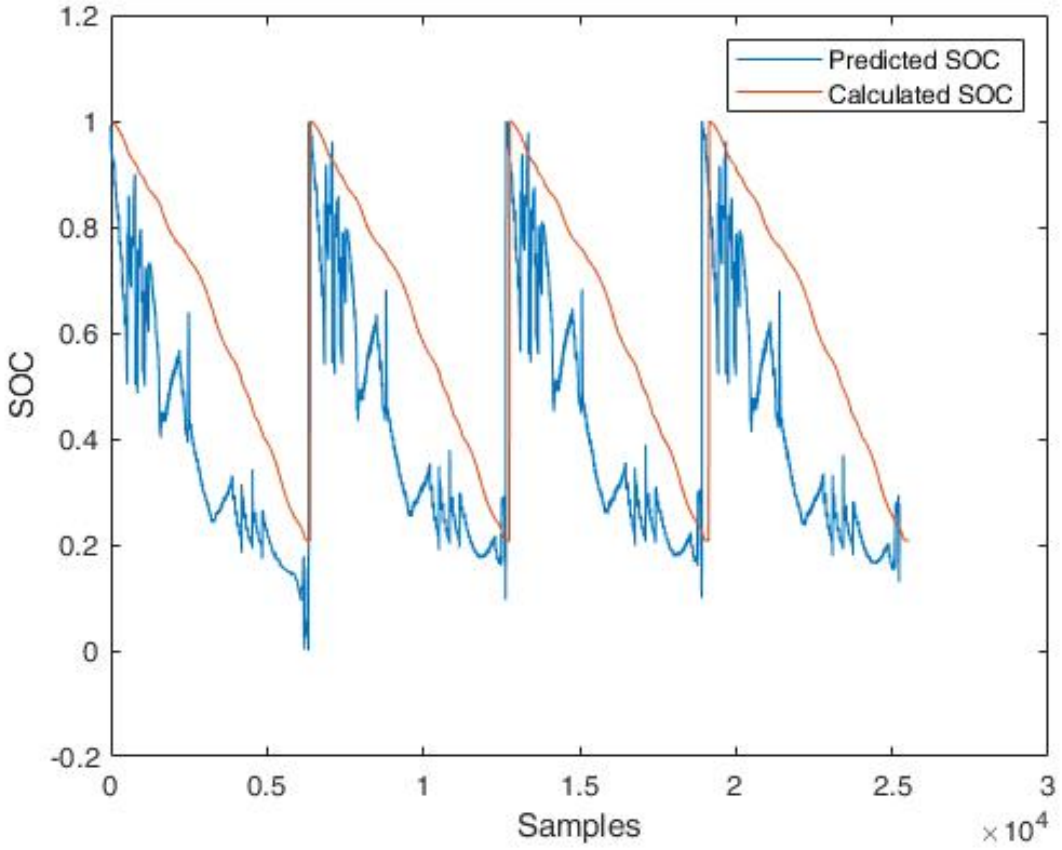

Figure 4.2: Estimated SOC by LG HG2 model

MAE has a value of 23.3%, the error between the real SOC computed by Coulomb Counting and the FNN estimation for each sample can be shown in figure 4.3:

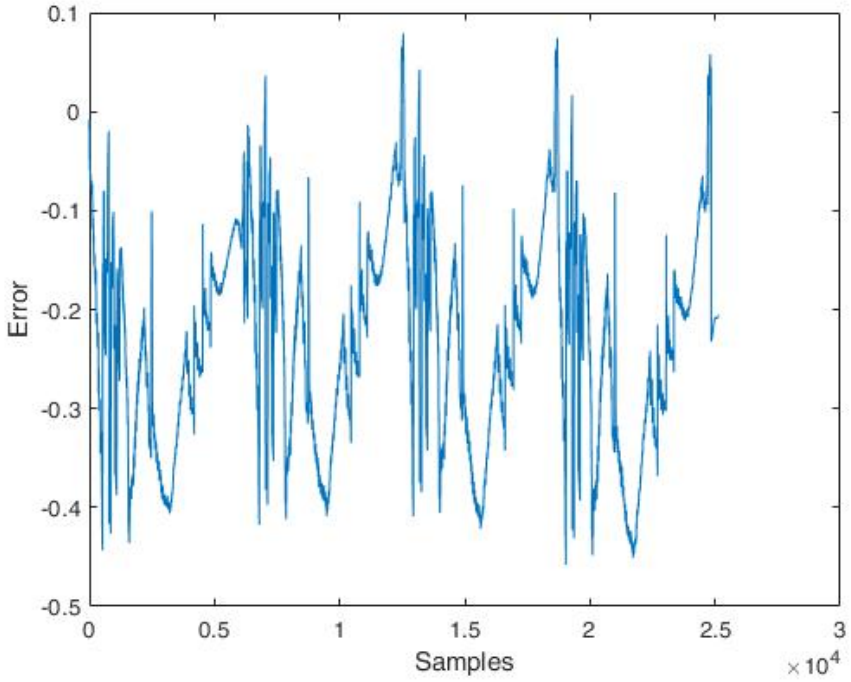

Figure 4.3: Error using LG HG2 model

4.2.2 Analyzing and Discussion

Figure 4.2 shows that the estimated SOC for the LG HG2 model differs significantly from the CGR18650CG model. This is because LG HG2 and CGR18650CG belong to different cell types with distinct characteristics. CGR18650CG is an LCO cell, while LG HG2 is an NMC cell. These differences in cell types lead to variations in internal impedance, causing the model to provide random SOC values due to the divergence between testing and training data.

Due to the substantial internal impedance in CGR18650CG, the estimated SOC tends to be lower than the calculated SOC, resulting in an underestimation of the true SOC value.

It is worth noting that both cell types initiate discharge with a voltage of 4.2V at 100% SOC and conclude at a voltage of 2.8V when reaching 20% SOC (cut-off voltage).

Furthermore, it is important to acknowledge that the sensors and experimental environment utilized in this test may introduce outliers, which can result in inaccurate predictions.

The significant error observed in SOC estimation can be primarily attributed to the variations in cell chemistry, physical characteristics (such as internal impedance), and the OCV curve.

Based on the analysis of Figure 4.2 and Figure 4.3, it can be concluded that modeling the behavior of lithium cells and accurately estimating SOC is a cell-specific task. Attempting to generalize the model and estimation process to other cell types would not be practically feasible.

4.3 CGR18650CG Model

To assess the ability of the model to learn from uncertain data and extract key features for estimating SOC, a series of constant current discharge tests were conducted on four CGR18650CG cells using the LG HG2 dataset as a reference. The discharge tests were carried out at different rates (0.25C, 0.5C, and 0.75C), and these results served as the training data. The objective was to determine if the model could effectively utilize high uncertainty data and accurately estimate SOC. Discharge tests were conducted using four cells connected in series, ensuring that they all experienced the same discharge current and depth of discharge. The resulting graphs from the four cells have been combined into a single figure, as shown below.

- Cell 01 : From0 to 0.625×10^4
- Cell 02 : From 0.625×10^4 to 1.25×10^4
- Cell 03 : From 1.25×10^4 to 1.875×10^4
- Cell 04 : From 1.875×10^4 to 2.5×10^4

Figure 4.4 illustrates the constant current discharge tests employed in this study.

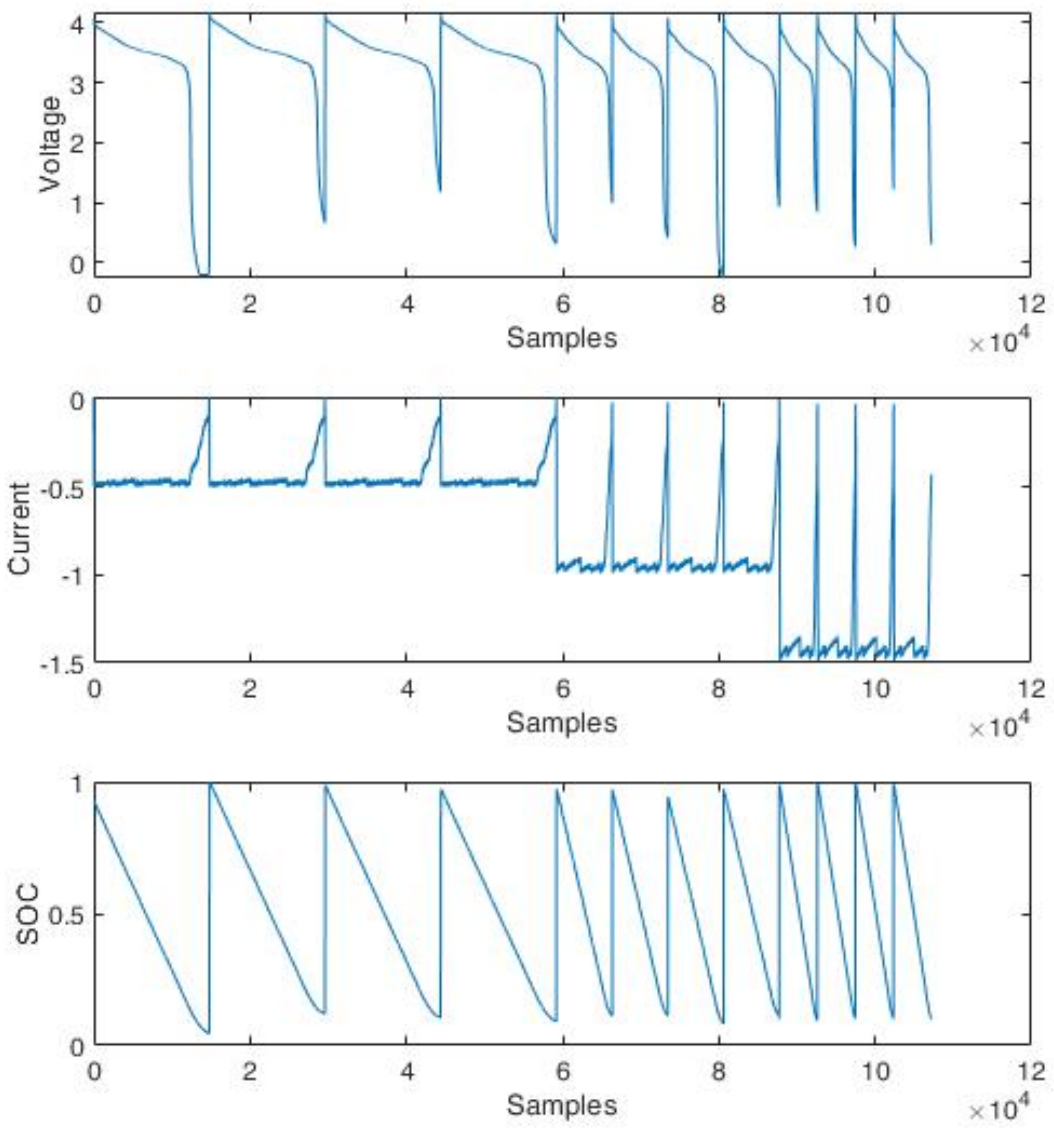

Figure 4.4: Constant Current Discharge Test for CGR18650CG Cell

4.3.1 Model Training and SOC Estimation

By Following same steps leading to training FNN model in Chapter 02, model training performances can be plotted as follows:

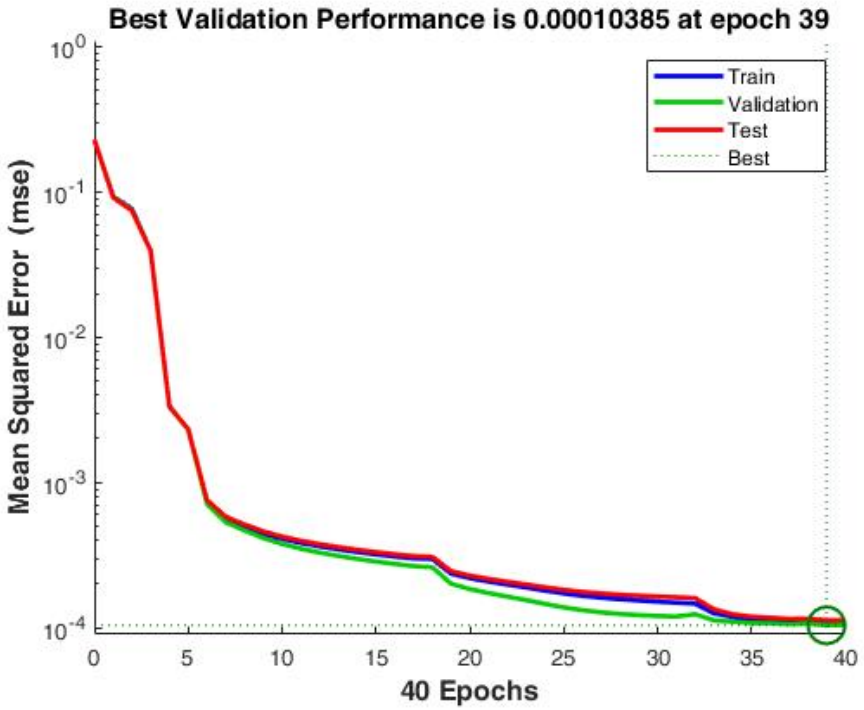

Figure 4.5: Mean Square Error

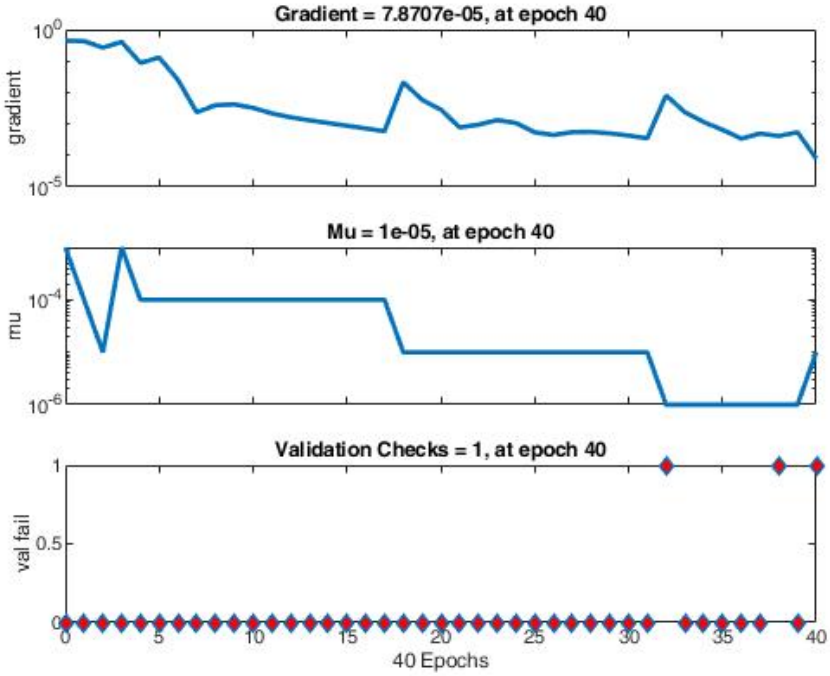

Figure 4.6: Training State

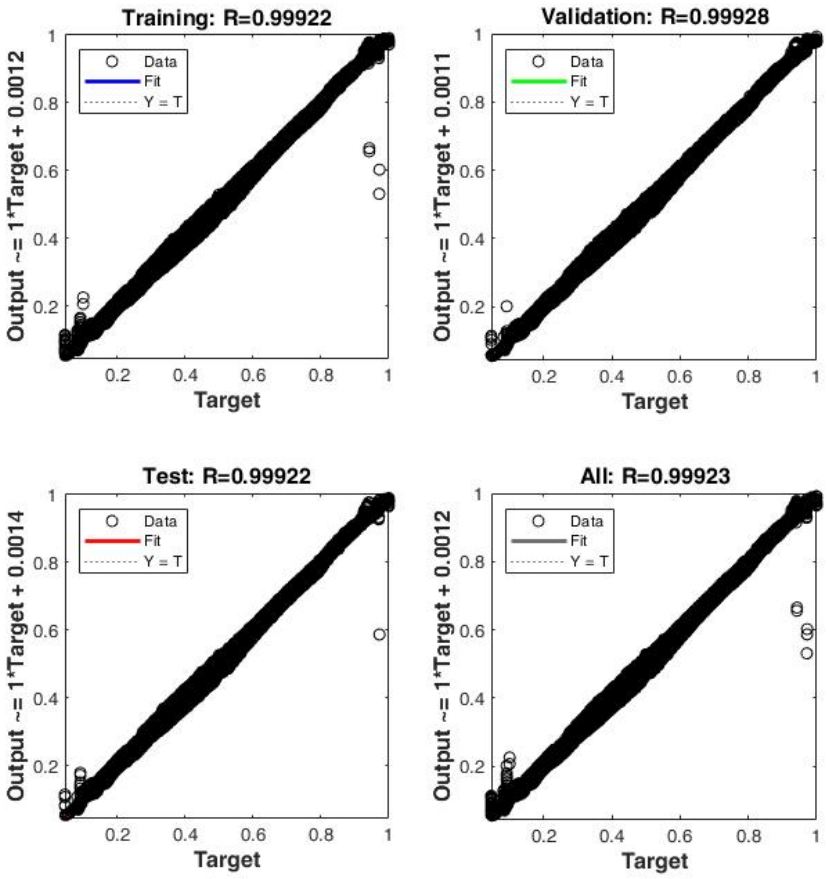

Figure 4.7: Regression Plot

After analyzing the graphs depicted in Figure 4.5 and Figure 4.7, a conclusion can be drawn that the mean squared error (MSE) of the validation data has mirrored the MSE of the training data. This indicates that there is no presence of underfitting or overfitting in the model. Additionally, by referring to Figure 4.6, it can be observed a consistent decrease in the gradient plot. This implies that the model is continuously making significant improvements. At epochs 18 and 32, the gradient temporarily increases due to a decrease in the learning rate. However, this adjustment allows the model to maintain a stable convergence.

By testing the model on data represented in Figure 4.1 the predicted SOC and error can be plotted respectively in Figures 4.8 and 4.9:

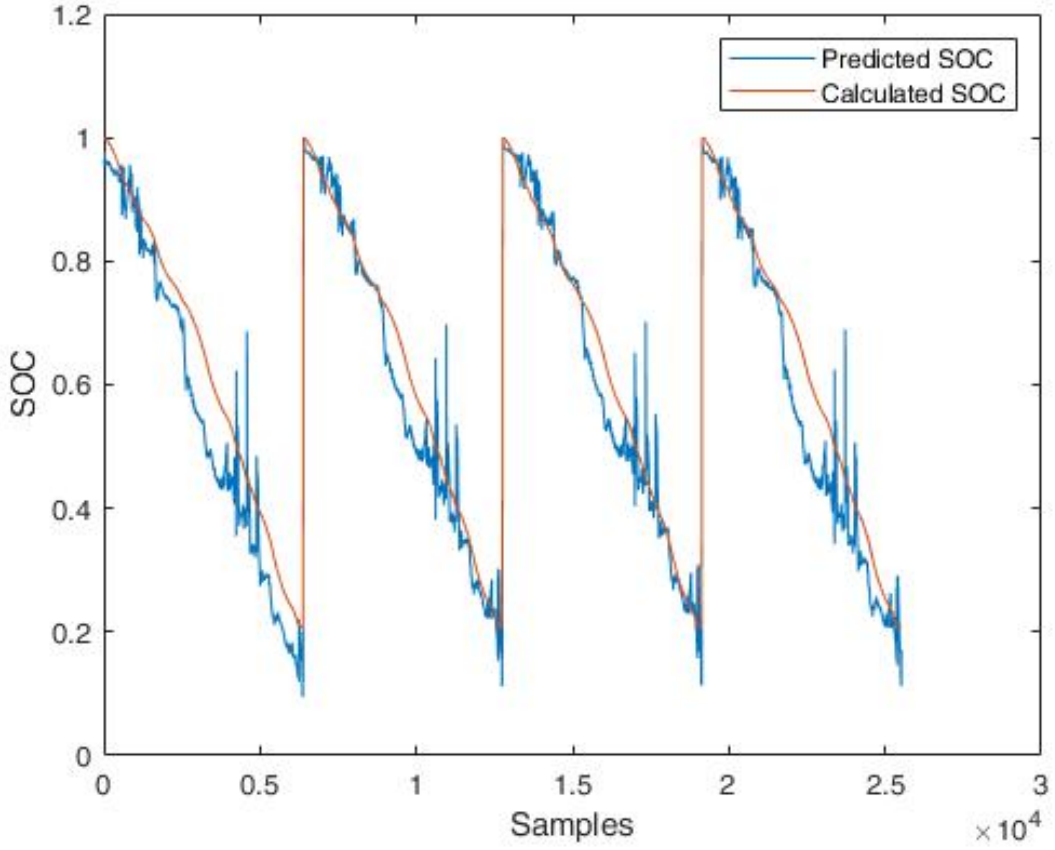

Figure 4.8: Predicted SOC vs Calculated SOC for CGR18650CG Model

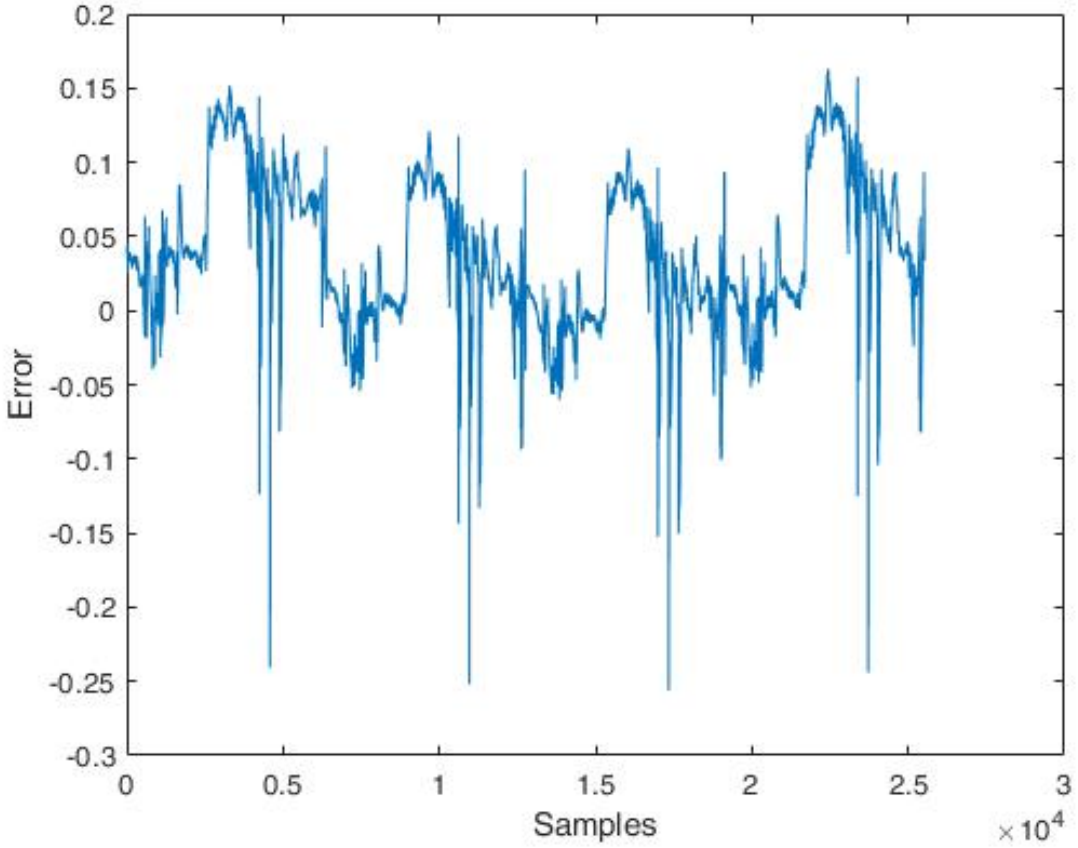

Figure 4.9: Error between Predicted and Calculated SOC

In order to eliminate noise, MAF has been applied on the estimated SOC to filter undesired pulses resulting from outliers. Figure 4.10 shows the filtered SOC vs the computed SOC.

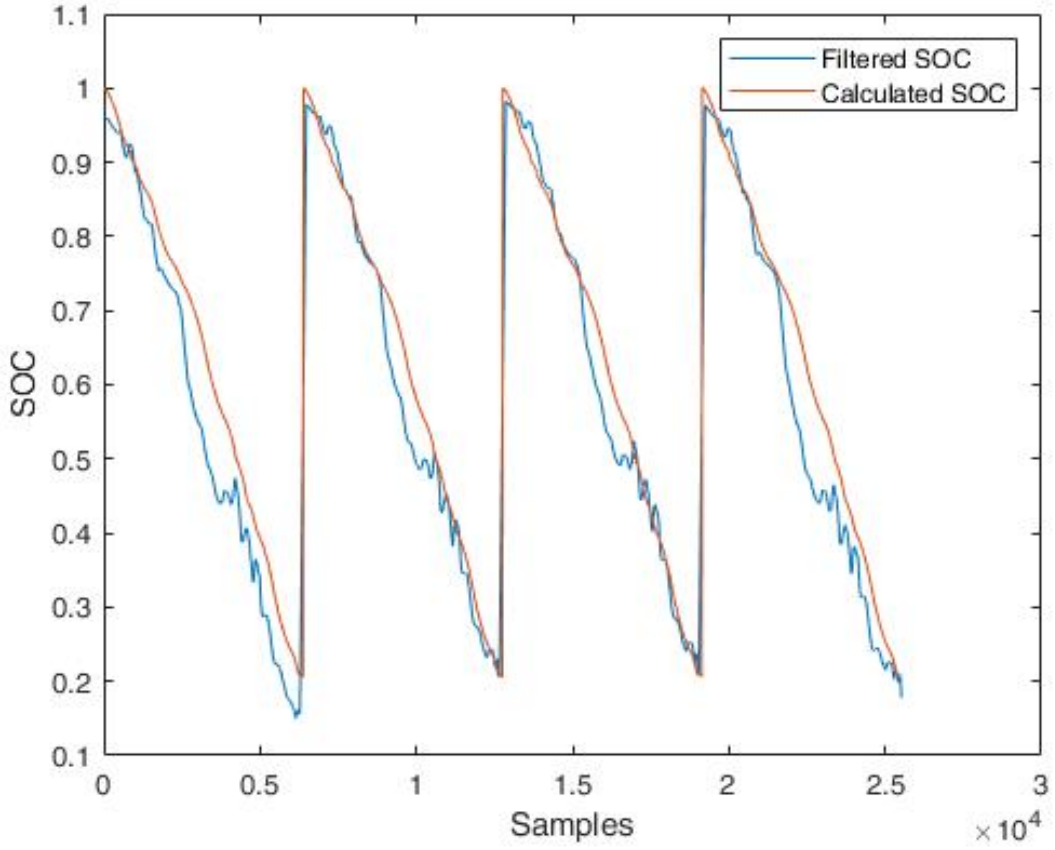

Figure 4.10: Filtered SOC vs Calculated SOC for CGR18650CG Model

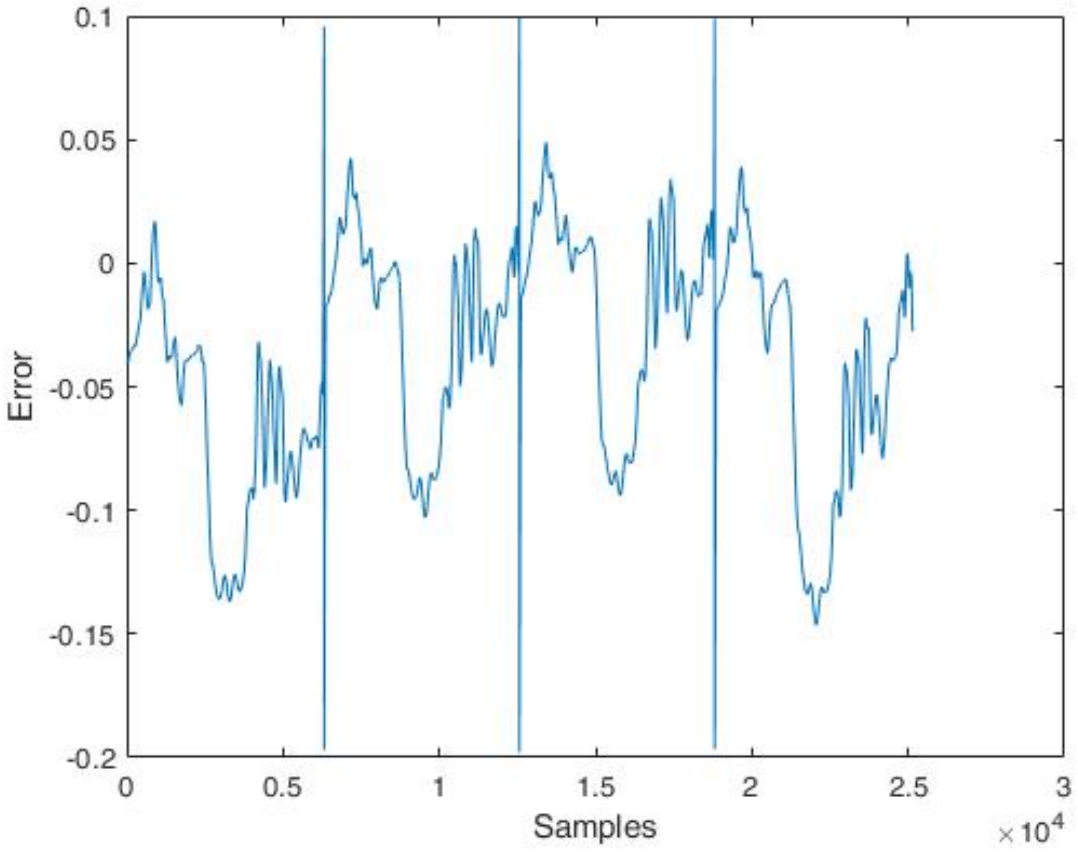

Figure 4.11: Error between Filtered and Calculated SOC

4.3.2 Analyzing and Discussion

First, the training data (Constant current discharge test) shows the terminal voltage decrease of the four cells, the three discharge current curves, and SOC calculated by coulomb counting. However, it can be noticed that cell 1 has a different behavior compared to the other cells, which is due to a short circuit that occurred accidentally during testing. This incident negatively affected the cell's health and increased its internal impedance.

Upon analyzing Figure 4.8, the estimated SOC is closer to the calculated SOC. At the beginning of discharge, the calculated SOC has been set at 100% by hypothesis, which is a drawback of the Coulomb Counting method.

Between SOC=70% to SOC=40%, the error is greater, indicating an underestimation

of the SOC by the model. This suggests that the internal impedance in constant current tests was higher than in this mixed test. Additionally, high noise is detected at 40% for all cells, which is due to outliers in the training data.

Above 70% and below 40%, the model provides good estimations, indicating that it has learned the features of the cells well within this SOC interval.

By applying MAF on the predicted SOC, the noise has been partially eliminated, achieving an MAE of 4.52% as shown in Figure 4.11. Also, cell 01 exhibits a distinct behavior with lower underestimation compared to the calculated SOC due to the accidental short circuit, which increased the internal impedance and caused a lower terminal voltage.

Overall, considering the sensors and experimental uncertainty, this model has successfully learned the features of the CGR18650CG lithium cell in constant current discharge only. However, the quality, quantity, and diversity of the data directly impact the network's ability to generalize and accurately solve the task at hand.

4.4 Conclusion

In this chapter, focusing on the implementation and results of the proposed SOC estimator model for the LG HG2 lithium cell. However, due to the unavailability of LG HG2 in the market, challenges in obtaining data for training and testing our model have been faced. As a substitute, a Panasonic CGR18650CG has been used in the experimental setup to explore the feasibility of training a model on LG HG2 to estimate the SOC of CGR18650CG.

By leveraging AI and advanced algorithms, the objectives were to address questions and considerations regarding the impact of cell variations on model performance and its real-world applications. limitations were encountered due to the unavailability of LG HG2, our approach provided insights into the potential implications of using CGR18650CG as a surrogate for SOC estimation. The findings are expected to contribute valuable insights to the field of battery management systems and aid in the development of accurate SOC

estimation techniques for future lithium cell applications.

Using the LG HG2 cell model, we achieved an impressive accuracy rate of 99% was achived by integrating the prediction function into the Arduino code. The collected results were transmitted to MATLAB in real-time for further off-time analysis, and the performance evaluation showed promising results. However, when comparing the estimated SOC by the LG HG2 model to the SOC calculated by Coulomb counting, a significant discrepancy was observed. This discrepancy can be attributed to the distinct characteristics and variations between LG HG2 and CGR18650CG cells, including differences in cell chemistry and internal impedance.

Furthermore, CGR18650CG model for SOC estimation by conducting constant current discharge tests. The model was trained on the LG HG2 dataset and demonstrated the ability to learn from uncertain data and accurately estimate SOC. However, some challenges were encountered, such as underestimation of SOC in certain SOC intervals and high noise due to outliers in the training data. By applying a moving average filter, the noise has been partially eliminated and achieved a Mean Absolute Error of 4.52%.

In general, our implementation and results highlight the importance of cell-specific modeling and the impact of variations in cell chemistry and physical characteristics on SOC estimation. The challenges and complexity accurately estimating SOC has been put forward, this task requires considering the specific features of each cell type. While our model successfully learned the features of the CGR18650CG lithium cell in constant current discharge, the quality, quantity, and diversity of the data significantly influence the model's ability to generalize and accurately estimate SOC.

General Conclusion and Prospects

Trough this study, we have observed the steps of developing an intelligent, flexible, embedded lithium battery state of charge estimator based on feed forward neural networks, capable of predicting the SOC by measuring the cell's terminal voltage, current, and temperature.

Accurate SOC estimation is a primary task for a battery management system. It enables effective energy management, prevents battery issues, and optimizes overall performance. With accurate SOC estimation, users can make informed decisions about energy consumption and avoid unexpected battery depletion. It also helps prevent overcharging and undercharging, ensuring the safety and longevity of the battery. Additionally, accurate SOC estimation allows for intelligent energy management strategies, maximizing energy utilization and efficiency.

To achieve these objectives, we have conducted extensive research on the dependencies of lithium cell behavior and SOC estimation requirements, with a focus on adapting the recent adaptive method of artificial intelligence to meet our needs.

It was also introduced the software and programming tools utilized in the implementation process. The Arduino Software, ISIS Proteus Software was employed for simulating sensors with Arduino, MATLAB Coder was used to convert a trained FNN model into an Arduino function, generating highly readable and portable code.

The electronic circuit section provided an overview of the electrical components used, including the Panasonic CGR18650CG Lithium Cell, Arduino Mega 2560, ACS712 Current Sensor Module, MP1584EN 12V Voltage Regulator, HX1314G 5V Voltage Regulator, and TP4056 Lithium Cell Charger Module. The circuit was implemented on a breadboard,

allowing developing an electronic circuit capable of measuring cell voltage and current, and estimating the SOC. We have highlighted the characteristics of these components and the steps followed in our project. Our project offers the following advantages:

- Accuracy: SOC can be estimated without depending on load consumption.
- Informed Energy Management: Accurate SOC estimation enables users to effectively monitor and manage available energy, making informed decisions regarding energy consumption and usage patterns.
- Avoid Unexpected Battery Depletion: Particularly important in applications like electric vehicles, accurate SOC estimation helps drivers plan their journeys and avoid unexpected battery depletion.
- Battery Safety and Longevity: Precise SOC estimation helps prevent overcharging, which can shorten battery life, and undercharging, which can lead to premature shutdowns.
- Autonomy: Lithium cells provide power supply for sensors and Arduino, making the circuit mobile.
- Flexibility: Can be integrated with laptops, mobile robots, and EVs, with low memory consumption in micro-controllers.

We are satisfied with our work but aim to further enhance the system. Here are some ideas and perspectives we have put forward to improve the system:

- Lithium cell testing environment : The Battery Tester creates a controlled environment for lithium cell testing, enabling precise measurement of voltage, current, temperature, energy, and power. It employs accurate sensors to ensure high precision during discharge/charge cycles under controlled temperature conditions.
- Adapting hybrid methods: further exploration of hybrid methods that combine multiple SOC estimation techniques could enhance accuracy and performance, for

example in our work using Kalman filter instead of MAE would probably give better results.

- Battery management system : the development of practical and efficient BMS that integrate accurate SOC, SOH and SOF estimation algorithms are important for optimizing battery performance and extending their lifespan.

Technology is advancing rapidly, and it is essential for us to stay updated and grasp all technological innovations and their real-world applications. This will enable us to keep pace with countries that are developing, utilizing, and commercializing these techniques.

Bibliography

[1] A. A. Chellal, J. Lima, J. Gonçalves, and H. Megnafi, *Battery management system for mobile robots based on an extended Kalman filter approch*. 2021, pp. 1131–1136.

[2] G. Ren, G. Ma, and N. Cong, "Review of electrical energy storage system for vehicular applications," *Renewable and Sustainable Energy Reviews*, vol. 41, pp. 225–236, 2015.

[3] C. Gong, Z. Xue, S. Wen, Y. Ye, and X. Xie, "Advanced carbon materials/olivine lifepo4 composites cathode for lithium ion batteries," *Journal of Power Sources*, vol. 318, pp. 93–112, 2016.

[4] M. Hannan, M. M. Hoque, A. Mohamed, and A. Ayob, "Review of energy storage systems for electric vehicle applications: Issues and challenges," *Renewable and Sustainable Energy Reviews*, vol. 69, pp. 771–789, 2017.

[5] J. Zhu, Y. Lu, C. Chen, *et al.*, "Porous one-dimensional carbon/iron oxide composite for rechargeable lithium-ion batteries with high and stable capacity," *Journal of Alloys and Compounds*, vol. 672, pp. 79–85, 2016.

[6] `https://www.dreamstime.com/`.

[7] F. Elmahdi, L. Ismail, and M. Noureddine, "Fitting the ocv-soc relationship of a battery lithium-ion using genetic algorithm method," in *E3S Web of Conferences*, EDP Sciences, vol. 234, 2021, p. 00 097.

[8] R. Tsiriry, "Etude de l'amelioration de la longevite de la performance des batteries lithium-ion pour voitures electriques," Ph.D. dissertation, Université d'Antananarivo, 2017.

[9] Y. Xing, W. He, M. Pecht, and K. L. Tsui, "State of charge estimation of lithium-ion batteries using the open-circuit voltage at various ambient temperatures," *Applied Energy*, vol. 113, pp. 106–115, 2014.

[10] C. Spanos, D. E. Turney, and V. Fthenakis, "Life-cycle analysis of flow-assisted nickel zinc-, manganese dioxide-, and valve-regulated lead-acid batteries designed for demand-charge reduction," *Renewable and Sustainable Energy Reviews*, vol. 43, pp. 478–494, 2015.

[11] M. Garcia-Plaza, D. Serrano-Jiménez, J. E.-G. Carrasco, and J. Alonso-Martinez, "A ni–cd battery model considering state of charge and hysteresis effects," *Journal of Power Sources*, vol. 275, pp. 595–604, 2015.

[12] Y. Zhu, W. H. Zhu, Z. Davis, and B. J. Tatarchuk, "Simulation of ni-mh batteries via an equivalent circuit model for energy storage applications," *Advances in Physical Chemistry*, vol. 2016, 2016.

[13] B. University, *BU-205: Types of Lithium-ion*, Accessed on 10 April 2023, 2019. [Online]. Available: `https://batteryuniversity.com/article/bu-205-types-of-lithium-ion`.

[14] R. M. Salgado, F. Danzi, J. E. Oliveira, A. El-Azab, P. P. Camanho, and M. H. Braga, "The latest trends in electric vehicles batteries," *Molecules*, vol. 26, no. 11, p. 3188, 2021.

[15] W.-Y. Chang, "The state of charge estimating methods for battery: A review," *International Scholarly Research Notices*, vol. 2013, 2013.

[16] D. Kim, K. Koo, J. J. Jeong, T. Goh, and S. W. Kim, "Second-order discrete-time sliding mode observer for state of charge determination based on a dynamic resistance li-ion battery model," *Energies*, vol. 6, no. 10, pp. 5538–5551, 2013.

[17] S. L. Storage. "Panasonic cgr18650cg datasheet." (), [Online]. Available: https://secondlifestorage.com/index.php?attachments/panasonic-cgr18650cg-pdf.1308/.

[18] H. Tian, P. Qin, K. Li, and Z. Zhao, "A review of the state of health for lithium-ion batteries: Research status and suggestions," *Journal of Cleaner Production*, vol. 261, p. 120 813, 2020.

[19] L. Song, Y. Zheng, Z. Xiao, C. Wang, and T. Long, "Review on thermal runaway of lithium-ion batteries for electric vehicles," *Journal of Electronic Materials*, vol. 51, no. 1, pp. 30–46, 2022.

[20] Y. Zhou, "Analysis of causes of fire and explosion of lithium battery and analysis of control measures," *Fire Prot. Today*, vol. 5, no. 04, pp. 126–127, 2020.

[21] W. Waag, C. Fleischer, and D. Sauer, "Critical review of the methods for monitoring of lithium-ion batteries in electric and hybrid vehicles," *Journal of Power Sources*, vol. 258, pp. 321–339, 2014.

[22] Battery University. "BU-808: How to Prolong Lithium-based Batteries." (), [Online]. Available: https://batteryuniversity.com/article/bu-808-how-to-prolong-lithium-based-batteries.

[23] G. L. Wu, "Study on the charge storage performance of li-ion battery," *Battery Bimon.*, vol. 04, pp. 275–277, 2007.

[24] B. Balagopal and M.-Y. Chow, "The state of the art approaches to estimate the state of health (soh) and state of function (sof) of lithium ion batteries," in *2015 IEEE 13th International Conference on Industrial Informatics (INDIN)*, IEEE, 2015, pp. 1302–1307.

[25] M. Naguib, P. Kollmeyer, and A. Emadi, "Lithium-ion battery pack robust state of charge estimation, cell inconsistency, and balancing," *Ieee Access*, vol. 9, pp. 50 570–50 582, 2021.

[26] Q. Lin, J. Wang, R. Xiong, W. Shen, and H. He, "Towards a smarter battery management system: A critical review on optimal charging methods of lithium ion batteries," *Energy*, vol. 183, pp. 220–234, 2019.

[27] S. Lee, J. Kim, J. Lee, and B.-H. Cho, "State-of-charge and capacity estimation of lithium-ion battery using a new open-circuit voltage versus state-of-charge," *Journal of Power Sources*, vol. 185, no. 2, pp. 1367–1373, 2008.

[28] A. Sidhu, A. Izadian, and S. Anwar, "Adaptive nonlinear model-based fault diagnosis of li-ion batteries," *IEEE Transactions on Industrial Electronics*, vol. 62, pp. 1002–1011, Feb. 2015. DOI: 10.1109/TIE.2014.2336599.

[29] H. Anbuky and P. Pascoe, "Vrla battery state-of-charge estimation in telecommunication power systems," *IEEE Transactions on Industrial Electronics*, vol. 47, no. 3, pp. 565–573, 2000.

[30] K. Bundy, M. Karlsson, G. Lindbergh, and A. Lundqvist, "An electrochemical impedance spectroscopy method for prediction of the state of charge of a nickel-metal hydride battery at open circuit and during discharge," *Journal of Power Sources*, vol. 72, no. 2, pp. 118–125, 1998.

[31] K. Movassagh, A. Raihan, B. Balasingam, and K. Pattipati, "A critical look at coulomb counting approach for state of charge estimation in batteries," *Energies*, vol. 14, no. 14, p. 4074, 2021.

[32] A. M. S. M. H. S. Attanayaka, J. P. Karunadasa, and K. T. M. U. Hemapala, "Estimation of state of charge for lithium-ion batteries - a review," *AIMS Energy*, vol. 7, no. 2, pp. 186–210, 2019. DOI: 10.3934/energy.2019.2.186.

[33] J. Bi, S. Shao, W. Guan, and L. Wang, "State of charge estimation of li-ion batteries in an electric vehicle based on a radial-basis-function neural network," *Chinese Physics B*, vol. 21, no. 11, p. 118 801, 2012.

[34] M. AZOUGGAGH. "Les différents systèmes d'irrigation." (consulté le 17 Décembre 2019), [Online]. Available: https://www.aqua6.info/blog/25_les-differents-systemes-d-irrigation.html.

[35] Y. Bengio, A. Courville, and P. Vincent, "Representation learning: A review and new perspectives," *IEEE Transactions on Pattern Analysis and Machine Intelligence*, vol. 35, no. 8, pp. 1798–1828, 2013. DOI: 10.1109/TPAMI.2013.50.

[36] J. G. Proakis and D. G. Manolakis, *Digital signal processing: Principles, algorithms, and edition*, 1995.

[37] "Arduino mega 2560 datasheet." (), [Online]. Available: https://store.arduino.cc/products/arduino-mega-2560-rev3.

[38] MathWorks, *MATLAB Coder*, https://www.mathworks.com/products/matlab-coder.html, Accessed: June 2023.

[39] "Acs712 current sensor datasheet." (), [Online]. Available: https://www.alldatasheet.es/datasheet-pdf/pdf/168326/ALLEGRO/ACS712.html.

[40] "Mp1584en voltage regulator module datasheet." (), [Online]. Available: https://www.utmel.com/components/mp1584en-step-down-converter-datasheet-pinout-and-circuit?id=241.

[41] "Hx1314g voltage regulator module datasheet." (), [Online]. Available: https://abra-electronics.com/voltage-regulator-modules/dc-dc-step-down-converters/psm-169.html.

[42] "Tp4056 cccv charger module datasheet." (), [Online]. Available: https://www.alldatasheet.fr/view.jsp?Searchword=TP4056.

Appendix A

Conceptual Implementation Arduino Code

```
#define variables; % V1, V2, V3, V4, current and Ah
#define functions and set parameters;

Void setup(){
Serial.begin(9600); % lanch serial 9600
long previous_time = 0;
}

Void loop(){

Read_analog_voltage();
normalize_voltage();
Read_analog_current();
normalize_current();
```

```
current_time = millis()/1000;
Ah = Ah + current*(current_time - previous_time)/(3600*2250);
% time is by seconds, we need to devide by 3600 to get it in hours
%and devide by the capacity to get DOD
previous_time = current_time;

%Send data to Serial to view them with MATLAB
Serial.println(voltages):
Serial.println(Current);
Serail.println(Ah);

SOC1 = MyNeuralNetwokFunction({V1, current, 0.5, V1, current});
SOC2 = MyNeuralNetwokFunction({V2, current, 0.5, V2, current});
SOC3 = MyNeuralNetwokFunction({V3, current, 0.5, V3, current});
SOC4 = MyNeuralNetwokFunction({V4, current, 0.5, V4, current});
% 0.5 is 25°C after normalization

delay(1000);

}
```

Appendix B

SOC Predicting Function

```
\text{#include "myNeuralNetworkFunction.h"}\\
\text{#include <math.h>}\\
double myNeuralNetworkFunction(const double x1[5]){
  static const double d_a[200] = {
      1.3506505425445658,   2.1322708479710326,    -0.42014459218790057,
      1.5773875475979788,   -0.36462908480459283,  3.4110935879032556,
      3.2752645252894634,   1.8489657962719186,    1.3060149403709371,
      2.4879703550308481,   -1.3572352056934216,   1.0631050406356819,
      0.24218372149629569,  0.53906299619105646,   0.25141244711437338,
      -1.5816295418869464,  2.0892132963096279,    -1.6463429576634718,
      -0.91414926066610425, 1.8653992452625858,    -3.0006769004511673,
      0.84400168064770886,  -1.699309886011102,    -1.177006228272528,
      1.1377784608416031,   -0.6967581057057407,   -1.5295390956715131,
      -0.54603259129514092, 1.6965211763655392,    -0.17408065512424364,
      0.23542046033180605,  -0.98198424248736371,  0.80283663769913738,
      1.4568300965943093,   -1.9361134101859989,   -1.6500993230894556,
      2.2244093671447609,   -2.6634856748398112,   0.6156256134721303,
      -0.42693237457653183, -1.5847178451173365,   0.47775278552210865,
      1.8294463243695736,   1.9268758466290641,    1.7241784842434209,
```

```
-1.2789745358424895,  -1.2502819909172138,  -0.76554403963937667,
-1.645687844916522,   -0.91039937163360685, -0.45857480753807428,
0.37825918913021872,  -1.1782212148527642,  -1.7800117408918992,
0.028675888059454219, 0.40058492755512,     0.17430867456462945,
0.92107124011071984,  0.33304763833888584,  1.1156070507621145,
0.957772946160816,    -0.58737931054309356, -1.9610533893771713,
-0.71947374627779115, -0.32874473787710784, 2.7874054384930624,
-0.46849237912749853, 2.1705994658120136,   0.2612531103644537,
-0.15458945876632996, -1.2834484500815455,  -1.2732728344426085,
1.4775063736011227,   -1.0909565573399882,  0.75925356206488737,
-1.3983252049516319,  -0.25263704146488436, 1.3759718131986365,
0.12679662740233369,  -0.82735706706731638, 1.4913415466142974,
1.4996052969166958,   -1.2350908202248241,  -1.4509737762999104,
-1.7614864789152094,  -0.38635327814875442, -0.65246906589954168,
-0.80507329465686217, 0.99299150407587333,  -0.20924967491011198,
-0.86088279505977616, 2.1736888689460163,   2.0351162570720396,
-1.5013988023055009,  2.4206480080401938,   1.4109338389053292,
1.4755178133021563,   -0.29297650136250808, -0.2141839481956726,
-1.0181274879690336,  -0.2350706085360898,  1.2413858148245269,
-0.884751267247794,   1.4304312475543284,   -1.5371268156529847,
0.20970963093154421,  -2.0857618294493658,  1.417605483481901,
0.76922788245122964,  -1.8939928487994213,  0.06214678157440847,
-0.20672757373323339, -0.018759187824259914, 0.80816877669216058,
-0.6192727736647875,  -1.2917354756612949,  0.46532625964497237,
-0.1169354265225671,  0.88416520645962837,  -1.4556512431242297,
-0.40180814038173385, -0.96245109914048665, 1.156454945280208,
-1.1301157538230167,  0.49080445814681217,  3.6358687816998487,
-2.1736773706789845,  -0.12743933689956885, -0.19797620298862117,
2.1661653849862605,   1.2368342484980883,   1.3554917993978639,
```

```
    1.1425852556556246,   1.4597513926227486,    -1.7483034639000548,
    2.3268899552729132,   0.33603077971399453,   1.1641863620084838,
    -2.5033532745701161,  -0.63855855867847711,  2.0023644189648877,
    2.0220774792718013,   0.78191111923205936,   2.0264360501562724,
    0.86532868706888966,  0.41750181915511797,   0.76685018964059981,
    0.91445771910423046,  0.32104792575112923,   1.9715416128208418,
    0.70992792696009788,  0.96566969694861537,   -0.95394133128681591,
    1.2032430220513077,   -2.5196205851135995,   1.5253316971058948,
    -1.5479746686129552,  1.4462396159618565,    -1.0674125477094873,
    0.99766557450128468,  0.77458993842585389,   1.1467441539243615,
    0.73744085782244506,  -0.57649342448174412,  0.69765547436610842,
    -0.85539529133580028, 0.16826582673676757,   -0.26977069429714351,
    -1.2112582632921511,  -0.474993205878015,    -0.992072691947093,
    1.0372911329522534,   -1.1935909693131384,   0.32339625685487444,
    0.96023402331222718,  -0.79193583819277413,  1.2824297965096989,
    -2.44282769180756,    0.42533262368177616,   0.58599921579392911,
    -0.53015206524310321, -1.4671865556080035,   -1.0297683384362952,
    -0.64332748769861059, 1.6791845265578673,    0.25416102804683893,
    0.11767799464482682,  0.668077885764157,     1.0675562866412485,
    -1.0222884964541923,  -1.8039050645716728,   -1.5966994175446085,
    1.8798279119820158,   -1.5963762022582109,   0.47241432510575554,
    -0.17676065606612437, -1.2564799862386751,   0.33725809300598847,
    2.4684106889768618,   0.67676665071456865};
static const double b_a[40] = {
    -0.73164838869580384,  0.11442937868847852,    0.31323376654811297,
    -0.031073664632704175, -0.39398728262804922,   0.45161657848436387,
    1.1419157696942326,    -1.1797171936824937,    0.63443040918465921,
    0.42361840992545285,   0.0927625492487639,     0.070061358261999551,
    -0.61481460930017862,  -0.0024206847899896039, 0.040956173083663241,
```

```
    -0.22112761653171004,  0.10292589185235594,    0.0944214036844272,
    -0.63748135748888757,  -0.058501343555859737,  0.53010911018469153,
    0.064989402104859054,  -0.0793573188650569,    0.30308668296712937,
    -0.022812175140580395, -0.060887305403575336,  0.052613919839953484,
    0.053964473036718134,  0.21464173260359382,    0.15602216924257539,
    -0.18119410049242277,  -0.71854696425439335,   -0.39179205501074232,
    0.061061733975980546,  0.14404002938075314,    0.12042385354975119,
    -0.14921915771680944,  -0.89809729840646624,   -0.13824279529582423,
    -0.23334803524524036};
static const double c_a[40] = {
    -3.2136626474686909,  -2.6618102328430915,  2.7230839852419173,
    -2.5010261475781337,  2.1666343982652019,   -4.9160095239202937,
    -1.7534392914285488,  -1.4934268224078608,  -1.2363408740721775,
    -1.6765713394517872,  1.5896498859274331,   -1.3477009624210003,
    -1.2708108203809509,  -1.510406570820547,   -0.82318576687956557,
    0.55538480397702494,  -0.31104500261873008, 0.91849893549435,
    -0.71097261739955953, -0.0905428003424755,  -0.11155859108307212,
    0.23195630674303813,  -0.16623915941420467, -1.395413203069763,
    0.64893916211075109,  -0.7400571435222949,  -0.67789362045050239,
    -0.98779331212822274, 1.1083658526574218,   -1.9746679802714779,
    2.3289159389989065,   -1.78498075007145,    2.0184204847705711,
    1.8568846931876781,   -1.4022952080565623,  -2.2753122279430209,
    2.4752702330929774,   -1.7680893728674876,  2.4479117593016637,
    -3.4468754239820103};
static const double dv[5] = {0.0, 0.0, 0.0, 0.172792340245624,
                             0.514377718585465};
static const double dv1[5] = {2.0, 2.0, 2.0, 2.52512947877986,
                              8.05598814106145};
double xp1[5];
```

```
double a;
double d;
int i;
int k;
/*  ===== NEURAL NETWORK CONSTANTS ===== */
/*  Input 1 */
/*  Layer 1 */
/*  Layer 2 */
/*  Output 1 */
/*  ===== SIMULATION ======== */
/*  Dimensions */
/*  samples */
/*  Input 1 */
/*  ===== MODULE FUNCTIONS ======== */
/*  Map Minimum and Maximum Input Processing Function */
for (k = 0; k < 5; k++) {
  xp1[k] = (x1[k] - dv[k]) * dv1[k] - 1.0;
}
/*  Layer 1 */
/*  Sigmoid Symmetric Transfer Function */
/*  Layer 2 */
/*  Output 1 */
/*  Map Minimum and Maximum Output Reverse-Processing Function */
a = 0.0;
for (k = 0; k < 40; k++) {
  d = 0.0;
  for (i = 0; i < 5; i++) {
    d += d_a[k + 40 * i] * xp1[i];
  }
```

```
    a += b_a[k] * (2.0 / (exp(-2.0 * (c_a[k] + d)) + 1.0) - 1.0);
  }
  return ((a - 0.5330429997250532) - -1.0) / 2.0;
}
void setup() {
%This is example for simulating the function
double inputs[5] = {0.6, 0.5, 0.5, 0.5, 0.5};
double result = myNeuralNetworkFunction(inputs);
Serial.begin(9600);
Serial.print("SOC: ");
Serial.println(result);
}

void loop() {
  // put your main code here, to run repeatedly:

}
```